Article

One-Step versus Stepwise Mechanism in Protonated Amino Acid-Promoted Electron-Transfer Reduction of a Quinone by Electron Donors and Two-Electron Reduction by a Dihydronicotinamide Adenine Dinucleotide Analogue. Interplay between Electron Transfer and Hydrogen Bonding

Junpei Yuasa, Shunsuke Yamada, and Shunichi Fukuzumi

J. Am. Chem. Soc., **2008**, 130 (17), 5808-5820 • DOI: 10.1021/ja8001452 • Publication Date (Web): 04 April 2008

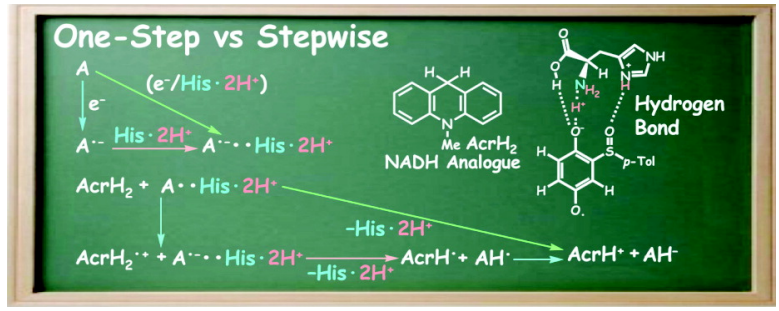

More About This Article

Additional resources and features associated with this article are available within the HTML version:

- Supporting Information
- Links to the 2 articles that cite this article, as of the time of this article download
- Access to high resolution figures
- Links to articles and content related to this article
- Copyright permission to reproduce figures and/or text from this article

View the Full Text HTML

J|A|C|S
ARTICLES

Published on Web 04/04/2008

One-Step versus Stepwise Mechanism in Protonated Amino Acid-Promoted Electron-Transfer Reduction of a Quinone by Electron Donors and Two-Electron Reduction by a Dihydronicotinamide Adenine Dinucleotide Analogue. Interplay between Electron Transfer and Hydrogen Bonding

Junpei Yuasa,† Shunsuke Yamada, and Shunichi Fukuzumi*

Department of Material and Life Science, Division of Advanced Science and Biotechnology, Graduate School of Engineering, Osaka University, SORST, Japan Science and Technology Agency (JST), Suita, Osaka 565-0871, Japan

Received January 8, 2008; E-mail: fukuzumi@chem.eng.osaka-u.ac.jp

Abstract: Semiquinone radical anion of 1-(*p*-tolylsulfinyl)-2,5-benzoquinone ($TolSQ^{\bullet-}$) forms a strong hydrogen bond with protonated histidine ($TolSQ^{\bullet-}$/His·$2H^+$), which was successfully detected by electron spin resonance. Strong hydrogen bonding between $TolSQ^{\bullet-}$ and His·$2H^+$ results in acceleration of electron transfer (ET) from ferrocenes [R_2Fc, R = C_5H_5, C_5H_4(*n*-Bu), C_5H_4Me] to TolSQ, when the one-electron reduction potential of TolSQ is largely shifted to the positive direction in the presence of His·$2H^+$. The rates of His·$2H^+$-promoted ET from R_2Fc to TolSQ exhibit deuterium kinetic isotope effects due to partial dissociation of the N−H bond in His·$2H^+$ at the transition state, when His·$2H^+$ is replaced by the deuterated compound (His·$2D^+$-d_6). The observed deuterium kinetic isotope effect (k_H/k_D) decreases continuously with increasing the driving force of ET to approach $k_H/k_D = 1.0$. On the other hand, His·$2H^+$ also promotes a hydride reduction of TolSQ by an NADH analogue, 9,10-dihydro-10-methylacridine ($AcrH_2$). The hydride reduction proceeds via the one-step hydride-transfer pathway. In such a case, a large deuterium kinetic isotope effect is observed in the rate of the hydride transfer, when $AcrH_2$ is replaced by the dideuterated compound ($AcrD_2$). In sharp contrast to this, no deuterium kinetic isotope effect is observed, when His·$2H^+$ is replaced by His·$2D^+$-d_6. On the other hand, direct protonation of TolSQ and 9,10-phenanthrenequinone (PQ) also results in efficient reductions of $TolSQH^+$ and PQH^+ by $AcrH_2$, respectively. In this case, however, the hydride-transfer reactions occur via the ET pathway, that is, ET from $AcrH_2$ to $TolSQH^+$ and PQH^+ occurs in preference to direct hydride transfer from $AcrH_2$ to $TolSQH^+$ and PQH^+, respectively. The $AcrH_2^{\bullet+}$ produced by the ET oxidation of $AcrH_2$ by $TolSQH^+$ and PQH^+ was directly detected by using a stopped-flow technique.

Introduction

Proton uptake and release often entail an improvement of the driving force of electron transfer (ET) in biological redox processes such as photosynthesis and respiration, which are essential for life.[1,2] When an electron acceptor (A) undergoes protonation (AH^+), the rate of ET is accelerated by the protonation.[3] Even when no protonation of A takes place, the rate of ET is accelerated by protonation of the resulting radical anion ($A^{\bullet-}$), which results in stabilization of the transition state as well as the ET product ($A^{\bullet-}$).[4] In such a case, the ET is coupled with protonation of $A^{\bullet-}$, that is, one-electron reduction and protonation of A occur at the same time (Scheme 1a green arrow). On the other hand, the promoting effects of H^+ on ET are often regulated by Brønsted bases (:B) such as amino acid residues in the protein environment.[5−8] In such a case, $A^{\bullet-}$ forms

Scheme 1

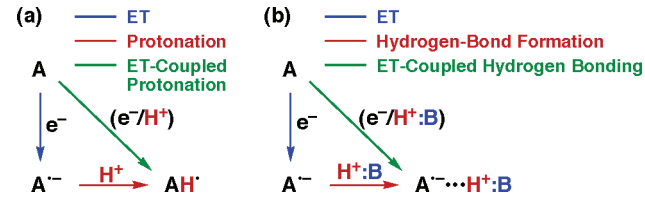

† Present address: Graduate School of Materials Science, Nara Institute of Science and Technology, 8916-5 Takayama, Ikoma, Nara 630-0192, Japan.

(1) (a) *The Photosynthetic Reaction Center*; Deisenhofer, J., Norris, J. R., Eds.; Academic Press: San Diego, CA, 1993. (b) *Anoxygenic Photosynthetic Bacteria*; Blankenship, R. E., Madigan, M. T., Bauer, C. E., Eds.; Kluwer Academic Publishing: Dordrecht, The Netherlands, 1995.
(2) (a) Kaim, W.; Schwederski, B. *Bioinorganic Chemistry: Inorganic Elements in the Chemistry of Life*; John Wiley & Sons: Chichester, U.K., 1994. (b) Ferguson-Miller, S.; Babcock, G. T *Chem. Rev.* **1996**, *96*, 2889.
(3) Fukuzumi, S. *Bull. Chem. Soc. Jpn.* **1997**, *70*, 1.
(4) (a) Fukuzumi, S.; Ishikawa, K.; Hironaka, K.; Tanaka, T. *J. Chem. Soc., Perkin Trans. 2* **1987**, 751. (b) Fukuzumi, S.; Mochizuki, S.; Tanaka, T *J. Am. Chem. Soc.* **1989**, *111*, 1497.
(5) Stowell, M. H. B.; McPhillips, T.; Rees, D. C.; Soltis, S. M.; Abresch, E.; Feher, G. *Science* **1997**, *276*, 812.
(6) Takahashi, E.; Wraight, C. A. *Biochemistry* **1992**, *31*, 855.
(7) Paddock, M. L.; Rongey, S. H.; Feher, G.; Okamura, M. Y. *Proc Natl. Acad. Sci. U.S.A.* **1989**, *86*, 6602.

10.1021/ja8001452 CCC: $40.75

a hydrogen bond with H^+:B instead of direct protonation, when :B acts as the stronger base than $A^{\bullet-}$ (Scheme 1b).[9–13] The interplay between ET and hydrogen bonding plays a crucial role in biological redox systems, for example, specific hydrogen bonds between nearby protonated amino acid residues and two quinones (termed Q_A and Q_B) determines the direction of an electron flow in photosynthetic reaction center.[14,15]

One may regard such H^+ and H^+:B-promoted ET as proton-coupled electron transfer (PCET). Although the precise definition of PCET has yet to be widely accepted,[16] this term is often applied to the mechanism in which the proton and electron are transferred in one single kinetic step.[17] It is therefore to be contrasted with the stepwise pathway that involves mechanistically distinct ET and proton transfer (PT) steps. The one-step pathway is generally thermodynamically more favorable than the stepwise pathway, because the one-step pathway avoids high-energy intermediates through the concerted electron–proton transfer.[16] Similarly, ET coupled with protonation (or hydrogen-bond formation) [Scheme 1 green arrows] should be thermodynamically more favorable than ET followed by protonation (or hydrogen-bond formation) [Scheme 1 red and blue arrows].[3,4] However, the one-step ET mechanism would be changed to the stepwise mechanism, when the driving force of the initial ET (Scheme 1 blue arrows) significantly increases. With regard to such a mechanistic dichotomy,[18] an important question arises: are both pathways employed simultaneously? Alternatively, is there a mechanistic continuity? However, such a mechanistic dichotomy, including the interplay between ET and hydrogen bonding (Scheme 1b), has yet to be scrutinized.

There is also a mechanistic dichotomy in hydride transfer of dihydronicotinamide adenine dinucleotide (NADH) and analogues, that is, one-step hydride transfer (green arrows) and ET followed by proton–electron (blue and red arrows) [or hydrogen (black arrows)] transfer as shown in Scheme 2.[19–22] NADH is an important source of two electrons and a proton in biological redox reactions,[23] and thereby always has been of general interest to chemists.[19–22,24–30] Hydride-transfer reactions of

Scheme 2

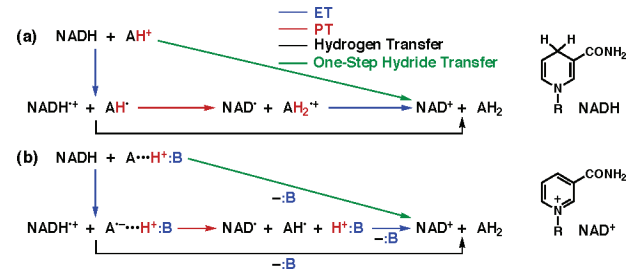

(8) Ädelroth, P.; Paddock, M. L.; Sagle, L. B.; Feher, G.; Okamura, M. Y. *Proc. Natl. Acad. Sci. U.S.A.* **2000**, *97*, 13086.

(9) For redox modulation by neutral hydrogen-bond donors, see: (a) Rotello, V. M. In *Electron Transfer in Chemistry*; Balzani, V., Ed.; Wiley-VCH: Weinheim, Germany, 2001; Vol. 4, pp 68–87. (b) Niemz, A.; Rotello, V. M. *Acc. Chem. Res.* **1999**, *32*, 44. (c) Greaves, M. D.; Niemz, A.; Rotello, V. M. *J. Am. Chem. Soc.* **1999**, *121*, 266. (d) Gray, M.; Cuello, A. O.; Cooke, G.; Rotello, V. M. *J. Am. Chem. Soc.* **2003**, *125*, 7882. (e) Jordan, B. J.; Pollier, M. A.; Miller, L. A.; Tiernan, C.; Clavier, G.; Audebert, P.; Rotello, V. M. *Org. Lett.* **2007**, *9*, 2835.

(10) Ammonium cations promote ET reductions of quinones by hydrogen-bond formation with semiquinone radical anions, see: Okamoto, K.; Ohkubo, K.; Kadish, K. M.; Fukuzumi, S. *J. Phys. Chem. A* **2004**, *108*, 10405.

(11) For effects of intramolecular hydrogen bonding on ET, see: (a) Rhile, I. J.; Markle, T. F.; Nagao, H.; DiPasquale, A. G.; Lam, O. P.; Lockwood, M. A.; Rotter, K.; Mayer, J. M. *J. Am. Chem. Soc.* **2006**, *128*, 6075. (b) Sjödin, M.; Irebo, T.; Utas, J. E.; Lind, J.; Merényi, G.; Åkermark, B.; Hammarström, L. *J. Am. Chem. Soc.* **2006**, *128*, 13076. (c) Costentin, C.; Robert, M.; Savéant, J.-M. *J. Am. Chem. Soc.* **2007**, *129*, 9953. (d) Fukuzumi, S.; Yoshida, Y.; Okamoto, K.; Imahori, H.; Araki, Y.; Ito, O. *J. Am. Chem. Soc.* **2002**, *124*, 6794. (e) Fukuzumi, S.; Okamoto, K.; Yoshida, Y.; Imahori, H.; Araki, Y.; Ito, O. *J. Am. Chem. Soc.* **2003**, *125*, 1007. (f) Okamoto, K.; Fukuzumi, S. *J. Phys. Chem. B.* **2005**, *109*, 7713.

(12) Extraordinarily large deuterium kinetic isotope effects were observed in a proton-coupled electron-transfer reaction of *p*-benzoquinone with an osmium complex containing a phosphorus-hydrogen bond; see: Huynh, M. H. V.; Meyer, T. J. *Proc. Natl. Acad. Sci. U.S.A* **2004**, *101*, 13138.

(13) For proton-coupled electron transfer in hydrogen-bonded donor-acceptor assemblies; see: (a) Roberts, J. A.; Kirby, J. P.; Nocera, D. G. *J. Am. Chem. Soc.* **1995**, *117*, 8051. (b) Kirby, J. P.; Roberts, J. A.; Nocera, D. G. *J. Am. Chem. Soc.* **1997**, *119*, 9230. (c) Hodgkiss, J. M.; Damrauer, N. H.; Pressé, S.; Rosenthal, J.; Nocera, D. G. *J. Phys. Chem. B* **2006**, *110*, 18853.

(14) (a) O'Malley, P. J. *J. Am. Chem. Soc.* **1998**, *120*, 5093. (b) O'Malley, P. J. *J. Phys. Chem. A* **1998**, *102*, 248.

(15) A part of preliminary results on direct ESR detection of a hydrogen-bonded complex between semiquinone radical anion of 1-(*p*-tolylsulfinyl)-2,5-benzoquinone and protonated histidine ($TolSQ^{\bullet-}$/$His\cdot 2H^+$) has appeared; see : Yuasa, J.; Yamada, S.; Fukuzumi, S. *Angew. Chem., Int. Ed.* **2007**, *46*, 3553.

(16) For various definitions and examples of PCET, see: (a) Mayer, J. M. *Annu. Rev. Phys. Chem.* **2004**, *55*, 363. (b) Cukier, R. I.; Nocera, D. G. *Annu. Rev. Phys. Chem.* **1998**, *49*, 337. (c) Kohen, A.; Klinman, J. P. *Acc. Chem. Res.* **1998**, *31*, 397. (d) Hammes-Schiffer, S . *Acc. Chem. Res.* **2001**, *34*, 273. (e) Stubbe, J.; Nocera, D. G.; Yee, C. S.; Chang, M. C. Y. *Chem. Rev.* **2003**, *103*, 2167. (f) Chang, C. J.; Chang, M. C. Y.; Damrauer, N. H.; Nocera, D. G. *Biochim. Biophys. Acta* **2004**, *1655*, 13. (g) Hammes-Schiffer, S. *ChemPhysChem* **2002**, *3*, 33. (h) Hammes-Schiffer, S. *Acc. Chem. Res.* **2006**, *39*, 93.

(17) Such concerted proton-electron transfer reactions have recently been termed as concerted proton-electron transfer (CPET); see: Costentin, C.; Evans, D. H.; Robert, M.; Savéant, J.-M.; Singh, P. S. *J. Am. Chem. Soc.* **2005**, *127*, 12490.

(18) For the mechanistic dichotomy between stepwise and concerted PCET, see: (a) Sjödin, M.; Styring, S.; Wolpher, H.; Xu, Y.; Sun, L.; Hammarström, L. *J. Am. Chem. Soc.* **2005**, *127*, 3855. (b) Lebeau, E. L.; Binstead, R. A.; Meyer, T. J. *J. Am. Chem. Soc.* **2001**, *123*, 10535. (c) Mayer, J. M.; Rhile, I. J *Biochim. Biophys. Acta* **2004**, *1655*, 51.

(19) (a) Fukuzumi, S.; Ishikawa, M.; Tanaka, T. *J. Chem. Soc., Perkin Trans. 2* **1989**, 1037. (b) Fukuzumi, S.; Mochizuki, S.; Tanaka, T. *J. Am. Chem. Soc.* **1989**, *111*, 1497. (c) Fukuzumi, S.; Ishikawa, M.; Tanaka, T. *Chem. Lett.* **1989**, 1227.

(20) (a) Carlson, B. W.; Miller, L. L *J. Am. Chem. Soc.* **1985**, *107*, 479. (b) Miller, L. L.; Valentine, J. R *J. Am. Chem. Soc.* **1988**, *110*, 3982.

(21) (a) Coleman, C. A.; Rose, J. G.; Murray, C. J. *J. Am. Chem. Soc.* **1992**, *114*, 9755. (b) Murray, C. J.; Webb, T. *J. Am. Chem. Soc.* **1991**, *113*, 7426.

(22) We have recently reported a mechanistic borderline between one-step and stepwise mechanisms in Sc^{3+}-promoted hydride transfer and hydrogen transfer of an NADH analogue; see: (a) Yuasa, J.; Yamada, S.; Fukuzumi, S. *J. Am. Chem. Soc.* **2006**, *128*, 14938. (b) Yuasa, J.; Fukuzumi, S. *J. Am. Chem. Soc.* **2006**, *128*, 14281.

(23) Stryer, L. *Biochemistry*, 3rd ed.; Freeman: New York, 1988; Chapter 17.

(24) (a) Fukuzumi, S.; Tanaka, T. *Photoinduced Electron Transfer*; Fox, M. A., Chanon, M., Eds.; Elsevier: Amsterdam, The Netherlands, 1988; Part C, Chapter 10. (b) Fukuzumi, S. *Advances in Electron Transfer Chemistry*; Mariano, P. S., Ed.; JAI Press: Greenwich, CT, 1992; pp 67–175.

(25) Gebicki, J.; Marcinek, A.; Zielonka, J. *Acc. Chem. Res.* **2004**, *37*, 379.

(26) (a) Eisner, U.; Kuthan, J. *Chem. Rev.* **1972**, *72*, 1. (b) Stout, D. M.; Meyers, A. I. *Chem. Rev.* **1982**, *82*, 223.

(27) (a) Pestovsky, O.; Bakac, A.; Espenson, J. H. *J. Am. Chem. Soc.* **1998**, *120*, 13422. (b) Pestovsky, O.; Bakac, A.; Espenson, J. H. *Inorg. Chem.* **1998**, *37*, 1616.

(28) Zhu, X.-Q.; Yang, Y.; Zhang, M.; Cheng, J.-P. *J. Am. Chem. Soc.* **2003**, *125*, 15298.

(29) For direct observation of $NADH^{\bullet+}$ analogues by the transient ESR spectrum in the oxidation of NADH analogues by *one-electron* oxidants, see: (a) Fukuzumi, S.; Tokuda, Y.; Kitano, T.; Okamoto, T.; Otera, J. *J. Am. Chem. Soc.* **1993**, 8960. (b) Fukuzumi, S.; Inada, O.; Suenobu, T. *J. Am. Chem. Soc.* **2003**, *125*, 4808.

NADH and analogues are often promoted by acids (H^+), when protonation of A (AH^+) enhances electrophilicity as well as the electron acceptor ability of A (Scheme 2a).[3,4,19–21] In the same way, the hydrogen-bond donor (H^+:B) would also promote hydride transfer of NADH and analogues via the one-step or stepwise pathways (Scheme 2b). Hydrogen-bond donors in the native enzymatic system, that is, the amino acid residues, play an important role in the redox reactions of nicotinamide coenzymes.[31] However, promoting effects of the hydrogen-bond donor on hydride transfer of NADH analogues through two distinct mechanisms have yet to be examined.

We report herein for the first time extensive analysis on a mechanistic dichotomy in a protonated histidine (His·$2H^+$)-promoted ET reduction of 1-(*p*-tolylsulfinyl)-2,5-benzoquinone (TolSQ) by electron donor as well as a two-electron reduction (formally hydride reduction) of TolSQ by an acid-stable NADH analogue, 9,10-dihydro-10-methylacridine ($AcrH_2$). The promoting effects of His·$2H^+$ on the ET and hydride-transfer reactions are also extensively compared with acid-promoted hydride reductions of TolSQ and 9,10-phenanthrenequinone (PQ) by $AcrH_2$.[32] We employed the protonated amino acid as a hydrogen-bond donor because of its important role in biological redox reactions (vide supra).[5–8,14,31,33,34] *p*-Quinone and *o*-quinone derivatives (TolSQ and PQ, respectively) are used as hydrogen-bond acceptors that have a multiple hydrogen-bonding site for His·$2H^+$.[35,36] The one-electron reduced species: a hydrogen-bonded complex of $TolSQ^{\bullet-}$ with His·$2H^+$ ($TolSQ^{\bullet-}$/His·$2H^+$), the semiquinone radical of TolSQ ($TolSQH^{\bullet}$), and the hydroquinone radical cation ($PQH_2^{\bullet+}$), were successfully detected by electron spin resonance (ESR).[15,32] Direct ESR detection of the ET products, combined with the extensive kinetic analysis of the His·$2H^+$-promoted ET and hydride transfer provides valuable insight into the mechanistic dichotomy in the His·$2H^+$-promoted ET reduction of the quinone as well as the two-electron reduction by an NADH analogue.

Experimental Section

Materials. 1-(*p*-Tolylsulfinyl)-2,5-benzoquinone (TolSQ) was prepared according to the literature.[37] Preparation of 10-methyl-9,10-dihydroacridine ($AcrH_2$) and the dideuterated compound ($AcrD_2$) was described previously.[38] The synthesis of 1-benzyl-1,4-dihydronicotinamide dimer [$(BNA)_2$] was also reported previously.[39] 10,10′-Dimethyl-9,9′-biacridine [$(AcrH)_2$] was prepared by the one-electron reduction of 10-methylacridinium perchlorate by hexamethylditin.[40] Histidine (His) was obtained from Aldrich. Perchloric acid [$HClO_4$] (70%) and deuterated $HClO_4$ ($DClO_4$) [66%] were also obtained from Aldrich. For safety reasons, $HClO_4$ (70%) containing 30% water was used in this work. Decamethylferrocene [$(C_5Me_5)_2Fc$] was obtained from Wako Pure Chemical Co., Ltd. 1,1′-Dimethylferrocene [$(C_5H_4Me)_2Fc$], 1,1′-di-*n*-butylferrocene ([$C_5H_4(n\text{-}Bu)]_2Fc$), and ferrocene [$(C_5H_5)_2Fc$] were obtained from Aldrich. 9,10-Phenanthrenequinone (PQ) was obtained commercially and purified by the standard methods.[41] Acetonitrile (MeCN) and propionitrile (EtCN) used as solvents were purified and dried by the standard procedure.[41] [$^2H_3$]Acetonitrile (CD_3CN) was obtained from EURI SO-TOP, CEA, France. [$^2H_2$]Water (D_2O) was purchased from Cambridge Isotope Laboratories. Tetra-*n*-butylammonium perchlorate (TBAP) was purchased from Fluka Chemical Co., twice recrystallized from absolute ethanol, and dried in a vacuum at 45 °C prior to use. Deuterated His·$2H^+$ (His·$2D^+$-d_6) was prepared by the following procedure: First, His (1.55 g) was dissolved in D_2O (50 mL) and stirred by the magnetic stirrer for 13 h. Then, deuterated His (His-d_4) was obtained by evaporation of the resulting aqueous solution. His·$2D^+$-d_6 was obtained by addition of 2 equiv of $DClO_4$ to a MeCN solution of His-d_4.

Reaction Procedures and Analysis. Typically, $AcrH_2$ (8.5×10^{-3} M) was added to an NMR tube that contained an [$^2H_3$]acetonitrile (CD_3CN) solution (0.6 mL) of TolSQ (8.5×10^{-3} M) in the presence of $HClO_4$ (3.0×10^{-2} M) under an atmospheric pressure of argon. Then the solution was deaerated with argon gas for 5 min, and the NMR tube was sealed with a rubber septum. The reaction was complete in one minute under these conditions. The products of hydride reductions of TolSQ and PQ ($TolSQH_2$ and PQH_2) were identified by comparing the ^1H NMR spectra with those in the literatures.[22a,42] The total yield of $TolSQH_2$ in the hydride-transfer reaction of TolSQ in the presence of $HClO_4$ and that in the presence of His·$2H^+$ were determined to be 97% and 98%, respectively, from the ^1H NMR spectra in comparison with the internal standard, 1,4-dioxane (2.0×10^{-2} M). The total yield of PQH_2 in the hydride-transfer reaction of PQ in the presence of $HClO_4$ was also determined to be 97% from the ^1H NMR spectra in comparison with the internal standard, 1,4-dioxane (2.0×10^{-2} M). ^1H NMR measurements were performed with a JMN-AL-300 (300 MHz) NMR spectrometer at 298 K.

Kinetic Measurements. Kinetic measurements were performed by using a UNISOKU RSP-601 stopped-flow spectrophotometer with an MOS-type high sensitive photodiode array. Rates of electron transfer from R_2Fc (1.0×10^{-4} M) to TolSQ (0 to 4.0×10^{-3} M) in the presence of His·$2H^+$ (0 to 5.0×10^{-2} M) and His·$2D^+$-d_6 (0 to 5.0×10^{-2} M) were monitored by the rise of the absorption band at 620 nm due to R_2Fc^+ in deaerated MeCN at 298 K. Rates of hydride transfer from $AcrH_2$ to TolSQ (0 to 2.0×10^{-3} M) in the presence of His·$2H^+$ (0 to 2.0×10^{-2} M) were monitored by an increase in the absorption band due to 10-methylacridinium ion

(30) For direct observation of sequential electron-proton transfer in *photoinduced* hydrogen transfer from NADH analogues to triplet species, **22b**, see: (a) Schaefer, C. G.; Peters, K. S. *J. Am. Chem. Soc.* **1980**, *102*, 7566. (b) Peters, K. S.; Pang, E.; Rudzki, J. *J. Am. Chem. Soc.* **1982**, *104*, 5535. (c) Manring, L. E.; Peters, K. S. *J. Am. Chem. Soc.* **1985**, *107*, 6452. (d) Peters, K. S.; Cashin, A.; Timbers, P. *J. Am. Chem. Soc.* **2000**, *122*, 107. (e) Dreyer, J.; Peters, K. S. *J. Phys. Chem.* **1996**, *100*, 19412.

(31) Brondijk, T. H. C.; van Boxel, G. I.; Singh, A.; Mather, O. M.; White, H. A.; Quirk, P. G.; White, S. A.; Jackson, J. B. *J. Biol. Chem.* **2006**, *281*, 13345.

(32) A part of preliminary results on direct detection of the radical cation of an NADH analogue, 9,10-dihydro-10-methylacridine ($AcrH_2$) has appeared; see: Yuasa, J.; Yamada, S.; Fukuzumi, S. *Angew. Chem., Int. Ed.* **2008**, *47*, 1068.

(33) It has been suggested that His-H126 and His-H128 nearby Q_B facilitate proton transfer into the RC; see: (a) Paddock, M. L.; Graige, M. S.; Feher, G.; Okamura, M. Y. *Proc. Natl. Acad. Sci. U.S.A.* **1999**, *96*, 6183. (b) Ädelroth, P.; Paddock, M. L.; Tehrani, A.; Beatty, J. T.; Feher, G.; Okamura, M. Y. *Biochemistry* **2001**, *40*, 14538.

(34) Muramoto, K.; Hirata, K.; Shinzawa-Itoh, K.; Yoko-o, S.; Yamashita, E.; Aoyama, H.; Tsukihara, T.; Yoshikawa, S. *Proc. Natl. Acad. Sci. U.S.A.* **2007**, *104*, 7881.

(35) (a) Ge, Y.; Lilienthal, R. R.; Smith, D. K. *J. Am. Chem. Soc.* **1996**, *118*, 3976. (b) Ge, Y.; Miller, L.; Ouimet, T.; Smith, D. K. *J. Org. Chem.* **2000**, *65*, 8831.

(36) Quinones act as biological electron acceptors that can undergo either one- or two-electron reductions coupled with protonation to yield the corresponding semiquinones and hydroquinones, respectively; see: *Functions of Quinones in Energy Conserving Systems*; Trumpower, B. I., Ed.; Academic Press: New York, 1986.

(37) (a) García Ruano, J. L.; Alemparte, C. *J. Org. Chem.* **2004**, *69*, 1405. (b) Carreño, M. C.; García Ruano, J. L.; Toledo, M. A.; Urbano, A. *Tetrahedron Lett.* **1994**, *35*, 9759. (c) Carreño, M. C.; García Ruano, J. L.; Lafuente, C.; Toledo, M. A. *Tetrahedron: Asymmetry* **1999**, *10*, 1119.

(38) Fukuzumi, S.; Koumitsu, S.; Hironaka, K.; Tanaka, T. *J. Am. Chem. Soc.* **1987**, *109*, 305.

(39) Wallenfels, K.; Gellerich, M. *Chem. Ber.* **1959**, *92*, 1406.

(40) Fukuzumi, S.; Kitano, T.; Mochida, K. *J. Am. Chem. Soc.* **1990**, *112*, 3246.

(41) Armarego, W. L. F.; Chai, C. L. L. *Purification of Laboratory Chemicals*, 5th ed.; Butterworth Heinemann: Amsterdam, The Netherlands, 2003.

(42) Calderazzo, F.; Forte, C.; Marchetti, F.; Pampaloni, G.; Pieretti, L. *Helv. Chim. Acta* **2004**, *87*, 781.

Scheme 3

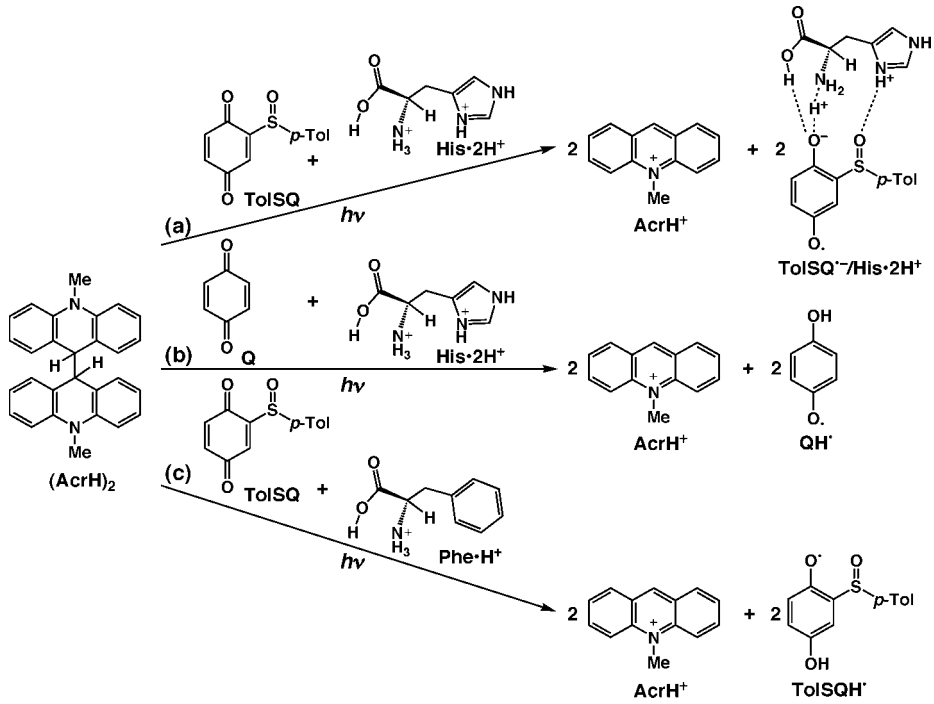

($AcrH^+$: $\lambda_{max} = 358$ nm, $\epsilon_{max} = 1.80 \times 10^4$ M^{-1} cm^{-1}) in deaerated MeCN at 298 K in the dark. All kinetic measurements were carried out under pseudo-first-order conditions where the concentrations of TolSQ were maintained at more than 10-fold excess of the concentrations of R_2Fc and $AcrH_2$ at 298 K. Pseudo-first-order rate constants were determined by least-squares curve fits using a personal computer.

ESR Measurements. ESR detection of $TolSQ^{\bullet-}$/His·$2H^+$, $TolSQH^{\bullet}$, and $PQH_2^{\bullet+}$ were performed as follows. Typically, TolSQ (8.0×10^{-3} M) was dissolved in deaerated MeCN and purged with argon for 10 min. His (8.0×10^{-3} M) and $HClO_4$ (1.6×10^{-2} M) were dissolved in deaerated MeCN. The TolSQ (200 μL) and His·$2H^+$ (200 μL) solutions were introduced into an ESR cell (1.8 mm i.d.) containing $(AcrH)_2$ (1.6×10^{-2} M) and mixed by bubbling with an Ar gas through a syringe with a long needle. The ESR spectra of $TolSQ^{\bullet-}$/His·$2H^+$, $TolSQH^{\bullet}$, and $PQH_2^{\bullet+}$ were recorded on a JEOL JES-RE1XE spectrometer under irradiation of a high pressure mercury lamp (USH-1005D) focusing at the sample cell in the ESR cavity. ESR detection of thermally generated $AcrH_2^{\bullet+}$ was performed by using a JEOL ES-EMCNT1 rapid mixing flow apparatus. Deaerated MeCN solutions of $AcrH_2$ (2.9×10^{-3} M) and TolSQ (2.8×10^{-3} M) in the presence of $HClO_4$ (7.0×10^{-2} M) under an atmospheric pressure of argon were mixed in a flat ESR cell at the flow rate of 1.9 cm^3 s^{-1}. The mixing time before reaching the ESR cell is about several hundred milliseconds, which is short enough to detect $AcrH_2^{\bullet+}$. The magnitude of modulation was chosen to optimize the resolution and signal-to-noise (S/N) ratio of the observed spectra under nonsaturating microwave power conditions. The *g* values were calibrated using an Mn^{2+} marker. Computer simulation of the ESR spectra was carried out by using Calleo ESR version 1.2 (Calleo Scientific Publisher) on a personal computer.

Cyclic Voltammetry. Cyclic voltammetry measurements were performed on a BAS 100W electrochemical analyzer in deaerated MeCN containing 0.1 M TBAP as a supporting electrolyte at 298 K. A conventional three-electrode cell was used with a platinum working electrode (surface area of 0.3 mm^2) and a platinum wire as the counter electrode. The Pt working electrode (BAS) was routinely polished with a BAS polishing alumina suspension and rinsed with acetone before use. The measured potentials were recorded with respect to the $Ag/AgNO_3$ (0.01 M) reference electrode. The second-harmonic alternating current voltammetry (SHACV) measurements of TolSQ (1.0×10^{-2} M) in the presence of His·$2H^+$ (5.0×10^{-3} M) and $HClO_4$ (1.0×10^{-2} M) were carried out with a BAS 100B electrochemical analyzer in deaerated MeCN containing 0.10 M TBAP as a supporting electrolyte at 298 K. All potentials (vs Ag/Ag^+) were converted to values vs SCE by adding 0.29 V.[43] All electrochemical measurements were carried out under an atmospheric pressure of argon.

Spectral Measurements. Protonation of TolSQ and PQ were examined from the UV–vis spectral changes of TolSQ (1.0×10^{-3} M) and PQ (1.0×10^{-3} M), respectively, in the presence of various concentrations of $HClO_4$ (0–1.4 M) by using a Hewlett-Packard 8453 diode array spectrophotometer.

Theoretical Calculations. Density-functional theory (DFT) calculations were performed on a 8CPU workstation (PQS, Quantum Cube QS8–2400C-064). Geometry optimizations were carried out using BeckeLYP functional and 6-31G** basis set[44] with the restricted Hartree–Fock (RHF) formalism or the unrestricted Hartree–Fock (UHF) and as implemented in the Gaussian 03 program, revision C.02.

Results and Discussion

ESR Detection of a Hydrogen-Bonded Complex between a Semiquinone Radical Anion and a Protonated Amino Acid. Hydrogen-bond formation of semiquinone radical anions with protonated amino acids were examined by ESR in photoinduced electron transfer (ET) from 10,10′-dimethyl-9,9′-biacridine [$(AcrH)_2$] to quinones (Scheme 3). The $(AcrH)_2$ is known to act as a two electron donor to produce 2 equiv of the radical anion of electron acceptor.[45] Steady-state photoirradiation of an acetonitrile (MeCN) solution of $(AcrH)_2$ (1.6×10^{-2} M) and 1-(*p*-tolylsulfinyl)-2,5-benzoquinone (TolSQ) (4.0×10^{-3}

(43) Mann, C. K.; Barnes, K. K. *Electrochemical Reactions in Nonaqueous Systems*; Marcel Dekker: New York, 1970.
(44) Becke, A. D. *J. Chem. Phys.* **1993**, *98*, 5648.
(45) (a) Fukuzumi, S.; Kitano, T.; Mochida, K. *J. Am. Chem. Soc.* **1990**, *112*, 3246. (b) Fukuzumi, S.; Tokuda, Y. *J. Phys. Chem.* **1992**, *96*, 8409.

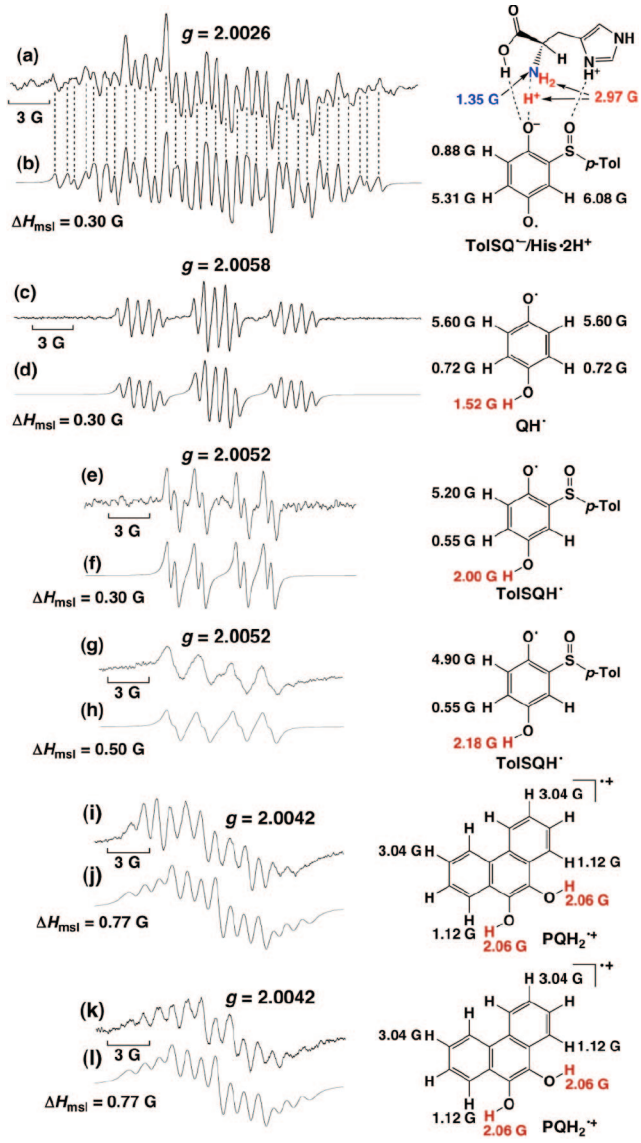

Figure 1. (a) ESR spectrum of a deaerated MeCN solution of TolSQ (4.0×10^{-3} M) and $(AcrH)_2$ (1.6×10^{-2} M) in the presence of His (4.0×10^{-3} M) and $HClO_4$ (8.0×10^{-3} M) under photoirradiation at 298 K and (b) the computer simulation spectrum. (c) ESR spectrum of a deaerated MeCN solution of Q (8.3×10^{-3} M) and $(AcrH)_2$ (1.6×10^{-2} M) in the presence of His (8.3×10^{-3} M) and $HClO_4$ (1.7×10^{-2} M) under photoirradiation at 298 K and (d) the computer simulation spectrum. (e) ESR spectrum of a deaerated MeCN solution of TolSQ (9.1×10^{-3} M) and $(AcrH)_2$ (1.6×10^{-2} M) in the presence of Phe (9.1×10^{-3} M) and $HClO_4$ (9.1×10^{-3} M) under photoirradiation at 233 K and (f) the computer simulation spectrum. (g) ESR spectrum of a deaerated EtCN solution of TolSQ (2.1×10^{-2} M) and $(BNA)_2$ (1.6×10^{-2} M) in the presence of $HClO_4$ (6.0×10^{-1} M) under photoirradiation at 193 K and (h) the computer simulation spectrum. (i) ESR spectrum of a deaerated EtCN solution of PQ (8.0×10^{-2} M) and $(BNA)_2$ (1.6×10^{-2} M) in the presence of His (5.2×10^{-1} M) and $HClO_4$ (1.04 M) under photoirradiation at 193 K and (j) the computer simulation spectrum. (k) ESR spectrum of a deaerated EtCN solution of PQ (5.0×10^{-2} M) and $(BNA)_2$ (1.6×10^{-2} M) in the presence of $HClO_4$ (2.5×10^{-2} M) under photoirradiation at 193 K and (l) the computer simulation spectrum.

M) in the presence of protonated histidine (His•2$HClO_4$) (4.0×10^{-3} M) afforded an ESR spectrum as shown in Figure 1a.[15,46]

Without steady-state photoirradiation, no ESR was detected because of instability of a hydrogen-bonded complex between $TolSQ^{\bullet-}$ and $His \cdot 2H^+$ ($TolSQ^{\bullet-}$/$His \cdot 2H^+$). The well-resolved ESR spectrum in Figure 1a allows us to determine the hyperfine coupling constants (hfc) due to three protons [a(3H) = 0.88, 5.31, and 6.08 G] of $TolSQ^{\bullet-}$ and superhyperfine splitting due to one nitrogen and three equivalent protons [a(N) = 1.35 G and a(3H) = 2.97 G] of $His \cdot 2H^+$ (Figure 1b). The complete agreement of the observed ESR spectrum (Figure 1a) with the computer simulation spectrum (Figure 1b) clearly indicates formation of the $TolSQ^{\bullet-}$/$His \cdot 2H^+$ complex (Scheme 3a). The g value (2.0026) and the hfc values [a(3H) = 0.88, 5.31, and 6.08 G] of the $TolSQ^{\bullet-}$/$His \cdot 2H^+$ complex are drastically changed from those of $TolSQ^{\bullet-}$ in the absence of $His \cdot 2H^+$, which are $g = 2.0057$ and a(3H) = 2.00, 2.20, and 3.35 G.[22a,47]

When p-benzoquinone (Q) is employed instead of TolSQ, only the protonated species (semiquinone radical: $QH^{\bullet}$) is detected by ESR in photoinduced ET from $(AcrH)_2$ to Q in the presence of $His \cdot 2H^+$ (Figure 1c, Scheme 3b). Similarly, only the semiquinone radical of TolSQ ($TolSQH^{\bullet}$) can be detected by ESR (Figure 1e), when $His \cdot 2H^+$ is replaced by protonated phenyl alanine ($Phe \cdot H^+$) (Scheme 3c).[48] Thus, the S=O oxygen in TolSQ as well as the N−H proton of imidazole ring in $His \cdot 2H^+$ play crucial roles for hydrogen-bond formation between $TolSQ^{\bullet-}$ and $His \cdot 2H^+$.[49] Virtually the same ESR spectrum as Figure 1e can be detected in photoinduced ET from dimeric 1-benzyl-1,4-dihydronicotinamide $[(BNA)_2]$[50] to TolSQ in the presence of $HClO_4$ (6.0×10^{-1} M) in propionitrile (EtCN) at 193 K (Figure 1g). In this case $(BNA)_2$ also acts as a two electron donor to produce 2 equiv of the semiquinone radical anions.[51,52] When the light is cut off, the ESR signal due to $TolSQH^{\bullet}$ disappears immediately as in the case of $TolSQ^{\bullet-}$/$His \cdot 2H^+$. This is attributed to a fast disproportionation of $TolSQH^{\bullet}$ ($2TolSQH^{\bullet} \rightarrow TolSQH_2 + TolSQ$). It should be emphasized that there is no ESR signal due to the diprotonated species, that is, $TolSQH_2^{\bullet+}$ even in the presence of the extremely high concentration of $HClO_4$ (6.0×10^{-1} M) (Figure 1g). This indicates that no further protonation of $TolSQH^{\bullet}$ takes place.

The optimized structure and the hfc values of $TolSQ^{\bullet-}$/$His \cdot 2H^+$ obtained by using density functional theory (DFT) at the BLYP/6–31G** basis are shown in Figure 2a.[53] The optimized structure of $TolSQ^{\bullet-}$/$His \cdot 2H^+$ shows multiple hydrogen bonding between $TolSQ^{\bullet-}$ and $His \cdot 2H^+$ (hydrogen bonds between the C=O oxygen of $TolSQ^{\bullet-}$ and the COOH

(46) Although His is hardly dissolved in MeCN, His becomes soluble in the presence of 2 equiv of $HClO_4$ in MeCN. Similarly, phenyl alanine (Phe) also becomes soluble in the presence of 1 equiv of $HClO_4$ in MeCN.

(47) The significantly smaller g value of $TolSQ^{\bullet-}$/$His \cdot 2H^+$ than $TolSQ^{\bullet-}$ (2.0057) indicates that the spin density on oxygen nuclei in $TolSQ^{\bullet-}$ is reduced significantly due to the strong hydrogen bonding with $His \cdot 2H^+$.

(48) Un-protonated His could not be employed as the control experiment, because His itself is hardly dissolved in MeCN (see ref 46).

(49) $His \cdot 2H^+$ acts as a multiple hydrogen-bond donor toward the semiquinone radical anion ($TolSQ^{\bullet-}$). Multiple hydrogen-bonds between nearby protonated amino acid residues and semiquinone radical anions play an important role in the direction of an electron flow in the photosynthetic reaction center. Nevertheless, $His \cdot 2H^+$ is less physiological as the carboxylate and amide are typically involved in peptide bonds.

(50) Patz, M.; Kuwahara, Y.; Suenobu, T.; Fukuzumi, S. *Chem. Lett.* **1997**, 567.

(51) Fukuzumi, S.; Suenobu, T.; Patz, M.; Hirasaka, T.; Itoh, S.; Fujitsuka, M.; Ito, O. *J. Am. Chem. Soc.* **1998**, *120*, 8060.

(52) The $(BNA)_2$ acting as stronger electron donor than $(AcrH)_2$ was used in the ESR detection of $TolSQH^{\bullet}$ (Figure 1g), because the $TolSQH^{\bullet}$ is quite unstable in the presence of extremely high concentration of $HClO_4$ (6.0×10^{-1} M). For the same reason, we employ $(BNA)_2$ in order to detect a hydroquinone radical cation of 9,10-phenanthrenequinone ($PQH_2^{\bullet+}$) by ESR (Figure 1, panels I and k).

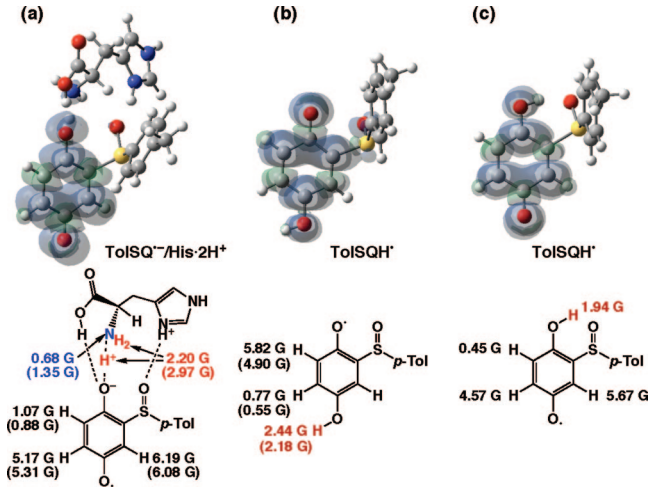

Figure 2. Optimized structures, spin-density plots, and the calculated hfc values of (a) TolSQ•−/His·2H+, (b) (c) TolSQH• calculated by using a density functional theory at the BLYP/6-31G** (observed hfc values are given in parentheses).

proton as well as the NH_3^+ protons of His·2H+, and also between the S=O oxygen of TolSQ•− and the NH^+ proton of the imidazole ring of His·2H+) [Figure 2a]. Such multiple hydrogen bonding may result in stabilization of TolSQ•−/His·2H+ (for the hydrogen-bond lengths; see Supporting Information S1).[54] The superhyperfine due to the hydrogen-bonded NH_3^+ proton of His·2H+ is estimated as 6.61 G. The averaged hfc value (2.20 G) due to the hydrogen-bonded NH_3^+ three protons agrees with the observed value (Figure 1b; parentheses in Figure 2a).[55] This indicates the rapid exchange in the NH_3^+ protons that is the hydrogen-bonded proton in the ESR time scale. The existence of the strong hydrogen bond between TolSQ•− and His·2H+ is firmly supported by the existence of the superhyperfine due to the hydrogen-bonded protons and nitrogen of NH_3^+ (Figure 1b). The optimized structures and the hfc values of TolSQH• are also obtained by DFT at the BLYP/6-31G** basis (Figures 2b and 2c).[53] The hfc values in Figure 2b agrees better with the observed values (Figure 1h and parentheses in Figure 2b) than those in Figure 2c.[55,56] Such agreement indicates that the proton from $HClO_4$ may be bound to the C=O oxygen on the opposite side of the S=O oxygen in contrast to the case of TolSQ•−/His·2H+.[57]

When 9,10-phenanthrenequinone (PQ) is employed as a multiple hydrogen-bond acceptor,[35] however, the diprotonated species (hydroquinone radical cation: $PQH_2^{\bullet+}$) is detected by ESR in photoinduced ET from $(BNA)_2$ to PQ in the presence of His·2H+ (Figure 1i) (Scheme 4).[52,58,59]

Formation of $PQH_2^{\bullet+}$ indicates the high basicity of monoprotonated species (PQH•), showing sharp contrast with the case of TolSQH• (vide supra). The ESR spectrum of $PQH_2^{\bullet+}$ is also detected by ESR in photoinduced ET from $(BNA)_2$ to PQ in the presence of a high concentration of $HClO_4$ (6.0×10^{-1} M) [Figure 1k].[52,60,61]

Large Positive Shifts in One-Electron Reduction Potentials of TolSQ and PQ in the Presence of His·2H+ or $HClO_4$. Strong hydrogen-bond formation between TolSQ•− and His·2H+ (TolSQ•−/His·2H+) as well as protonation of TolSQ•− (TolSQH•) are expected to result in positive shifts of the one-electron reduction potential (E_{red}) of TolSQ,[9,10] which were verified by the electrochemical measurements (vide infra). In contrast to a reversible redox wave of TolSQ in the absence of His·2H+ (or $HClO_4$) [Figure 3a], the cyclic voltammogram of TolSQ in the presence of His·2H+ (Figure 3b)[15] and that in the presence of $HClO_4$ (Figure 3d) exhibit irreversible cathodic waves due to instability of TolSQ•−/His·2H+ and TolSQH•, respectively. Thus, the E_{red} value of TolSQ in the presence of His·2H+ and the value in the presence of $HClO_4$ were determined by second-harmonic alternating current voltammetry (SHACV) [Figure 3c and 3e, respectively]. In the presence of 5.0×10^{-2} M of His·2H+, the E_{red} value of TolSQ (−0.26 V versus SCE) is shifted to 0.29 V versus SCE (Figure 3c),[15] which is further shifted to 0.69 V versus SCE in the presence of 5.0×10^{-2} M of $HClO_4$ (Figure 3e).[32]

Since the formation constants of TolSQ/His·2H+ and $TolSQH^+$ are significantly smaller than those of the one-electron reduced products, TolSQ•−/His·2H+ (K_1) and TolSQH• (K_2), the positive shift in the one-electron reduction potential of TolSQ in the presence of His·2H+ and that in the presence of $HClO_4$ are expressed by eq 1 and 2, respectively, where E^0_{red} is the reduction potential of TolSQ in the absence of His·2H+ (or $HClO_4$). The K_1 and K_2 values were determined as 4.2×10^{10} M^{-1} and 2.5×10^{17} M^{-1} from the E_{red} value of TolSQ in the presence of His·2H+ (5.0×10^{-2} M) and the value in the presence of $HClO_4$ (5.0×10^{-2} M), respectively. Such large K_1 and K_2 values indicate the existence of strong hydrogen

$$E_{red} = E^0_{red} + (2.3RT/F)\log\{K_1[\text{His}\cdot 2H^+]\} \quad (1)$$

$$E_{red} = E^0_{red} + (2.3RT/F)\log\{K_2[H^+]\} \quad (2)$$

(53) The calculated hfc values of semiquinone radical (QH•) by using BLYP methods have been reported to agree well with experimental data, see: Nonella, M. *J. Phys. Chem. B* **1997**, *101*, 1235.

(54) The hydrogen-bonded proton of NH_3^+ is not covalently bound to TolSQ•− but electrostatically bound to TolSQ•− through the hydrogen bond. The distance of the N-H bond in NH_3^+ (1.57 Å) is longer than that between the NH_3^+ proton and the C=O oxygen of TolSQ•− (1.05 Å) in the optimized structure of TolSQ•−/His·2H+ (see Supporting Information S2). This indicates that the binding of the N-H bond in NH_3^+ is significantly weakened by strong hydrogen-bond formation with TolSQ•−.

(55) Some deviations of the calculated hfc values of TolSQ•−/His·2H+ (Figure 2a) and TolSQH• (Figure 2b) from those of observed values (Figures 1b and 1h, respectively) indicate that the spin distribution is somewhat affected by the solvent.

(56) The ESR-measured hfc values (parentheses in Figure 2b) for TolSQH• are ***not*** an average of the DFT-determined values for b and c in Figure 2, because two large hfc values [a(2H) = 4.57 and 5.67 G] due to two protons in Figure 2c are inconsistent with the existence of only one large hfc value [a(H) = 4.90 G] due to one proton (parentheses in Figure 2b).

(57) The structure of TolSQH• in Figure 2c is enthalpically more favorable but entropically less favorable than that in Figure 2b. This may be the reason why H+ binds to the C=O oxygen on the opposite side of the S=O oxygen as shown in Figure 2b in which the C=O oxygen far from the S=O oxygen is involved.

(58) The existence of two protons binding to two C=O oxygens in $PQH_2^{\bullet+}$ was confirmed by a drastic change of the ESR spectrum (Figure 1i) by deuterium substitution of $HClO_4$ by $DClO_4$ (see Supporting Information S2). This affords a clear assignment of the observed hfc values of $PQH_2^{\bullet+}$, because a single deuteron gives a triplet (instead of doublet) hyperfine pattern and the deuteron splitting should decrease by the magnetogyric ratio of proton to deuterium (0.153).

(59) We have previously reported the 1:2 complex between PQ•− and La^{3+} [PQ•−-(La^{3+})$_2$]; see: Yuasa, J.; Suenobu, T.; Fukuzumi, S. *ChemPhysChem* **2006**, *7*, 942.

(60) The ESR spectrum due to $PQH_2^{\bullet+}$ (Figure 1k) is changed to PQH• in the presence of a low concentration of $HClO_4$ (2.5×10^{-2} M) (see Supporting Information S3).

(61) For ESR spectra of *o*-semiquinone radicals, see: (a) Lucarini, M.; Mugnaini, V.; Pedulli, G. F. *J. Org. Chem.* **2002**, *67*, 928. (b) Ci, X.; da Silva, R. S.; Nicodem, D.; Whitten, D. G. *J. Am. Chem. Soc.* **1989**, *111*, 1337.

Scheme 4

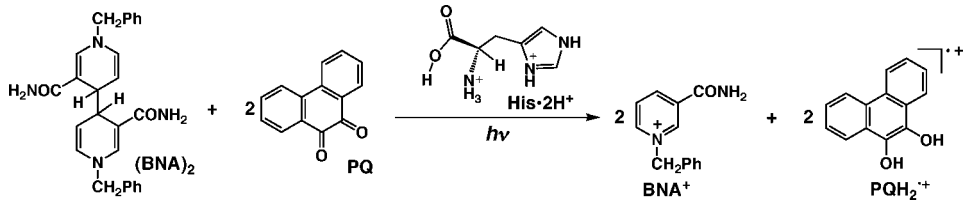

bonding in $TolSQ^{\bullet-}$/His·$2H^+$ and the high basicity of $TolSQ^{\bullet-}$, respectively. Similarly, the E_{red} value of PQ in the presence of $HClO_4$ was determined by SHACV (Figure 3g), because the cyclic voltammogram of PQ in the presence of $HClO_4$ also exhibits an irreversible cathodic wave due to the instability of $PQH_2^{\bullet+}$ (Figure 3f). The E_{red} value of PQ (−0.65 V versus SCE)[59] is shifted to 0.51 V versus SCE in the presence of 5.0×10^{-2} M $HClO_4$ (Figure 3g). The significant positive shift of the E_{red} value of PQ (+1.16 V) in the presence of $HClO_4$ (4.9×10^{-2} M) indicates that $PQ^{\bullet-}$ is significantly stabilized by diprotonation to form $PQH_2^{\bullet+}$ (see the ESR spectrum in Figure 1k).

His·$2H^+$-Promoted ET from R_2Fc to TolSQ. The positive shift of the E_{red} value of TolSQ in the presence of His·$2H^+$ (Figure 3c) should result in enhancement of the reactivity of the ET reduction of TolSQ, which was examined by ET from ferrocenes (R_2Fc) to TolSQ in the presence of His·$2H^+$ (vide infra). Since the free-energy change of ET from 1,1′-dimethylferrocene [$(C_5H_4Me)_2Fc$] (E_{ox} = 0.26 V vs SCE) to TolSQ (E_{red} = –0.26 V vs SCE)[22a] in the absence of His·$2H^+$ is highly endergonic (ΔG^0_{et} = 0.52 eV), no ET reaction occurs in the absence of His·$2H^+$. In the presence of His·$2H^+$ (5.0×10^{-2} M), however, the E_{red} value of TolSQ is shifted to 0.29 V vs SCE (vide supra). ET from $(C_5H_4Me)_2Fc$ to TolSQ therefore occurs in the presence of His·$2H^+$ (eq 3), as expected from the negative free-energy change of ET (ΔG_{et} = –0.03 eV).

The rates of His·$2H^+$-promoted ET from $(C_5H_4Me)_2Fc$ to

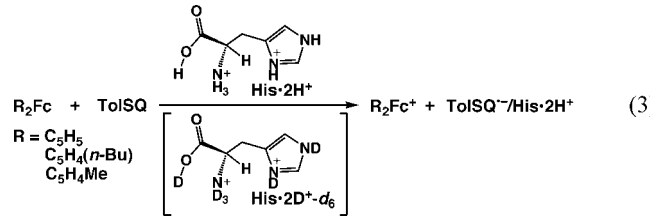

(3)

TolSQ obeyed pseudo-first-order kinetics in the presence of a large excess TolSQ and His·$2H^+$ relative to the concentration of $(C_5H_4Me)_2Fc$ (see the first-order plot in Supporting Information S4). The observed pseudo-first-order rate constant (k_{obs}) increases proportionally with increasing TolSQ concentration (see Supporting Information S5). The second-order rate constant (k_H) also increases linearly with increasing the His·$2H^+$ concentration ([His·$2H^+$]) [Figure 4a red circles].[15] Virtually the same results are obtained, when ferrocene [$(C_5H_5)_2Fc$] (E_{ox} = 0.37 V versus SCE) and 1,1′-di-*n*-butylferrocene ([C_5H_4(*n*-Bu)]$_2$Fc) [E_{ox} = 0.31 V vs SCE] are employed instead of $(C_5H_4Me)_2Fc$ (red circles in Figures 4b and 4c, respectively; see Supporting Information S5).[62]

$$\Delta G_{et} = \Delta G^0_{et} - (2.3RT/F)\log\{K_1[\text{His}\cdot 2H^+]\} \qquad (4)$$

Since His·$2H^+$ has no effect on the oxidation potential of R_2Fc, the free energy change of ET from R_2Fc to TolSQ in the presence of His·$2H^+$ (ΔG_{et}) can be expressed by eq 4, where ΔG^0_{et} is the free energy change in the absence of His·$2H^+$. Such a change in ΔG_{et} has previously been well evaluated in light of the Marcus theory of ET[63] for metal ion-promoted ET from ferrocene to naphthoquinone (NQ) moiety of ferrocene-naphthoquinone (Fc-NQ) linked dyad, when the second-order rate constant of ET (k_{et}) increases linearly with increasing the concentration of metal ion.[64] In the same way, the k_H value also increases linearly with [His·$2H^+$] in His·$2H^+$-promoted

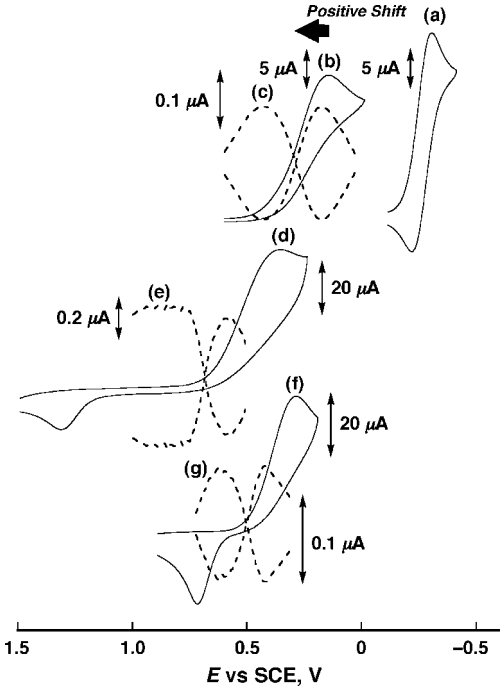

Figure 3. (a) Cyclic voltammogram of TolSQ (1.0×10^{-2} M) in the absence of His·$2H^+$, (b) cyclic voltammogram and (c) second-harmonic alternating current voltammogram of TolSQ (5.0×10^{-3} M) in the presence of His·$2H^+$ (5.0×10^{-2} M) in deaerated MeCN containing tetra-*n*-butylammonium perchlorate (TBAP) [0.10 M] with Pt working electrode at 298 K; sweep rate 0.1 V s^{-1}. (d) Cyclic voltammogram and (e) second-harmonic alternating current voltammogram of TolSQ (5.0×10^{-3} M) in the presence of $HClO_4$ (5.0×10^{-2} M) in deaerated MeCN containing TBAP (0.10 M) with Pt working electrode at 298 K; sweep rate 0.1 V s^{-1}. (f) Cyclic voltammogram and (g) second-harmonic alternating current voltammogram of PQ (7.0×10^{-3} M) in the presence of $HClO_4$ (5.0×10^{-2} M) in deaerated MeCN containing TBAP (0.10 M) with Pt working electrode at 298 K; sweep rate 0.1 V s^{-1}.

(62) Although ET from $(C_5H_5)_2Fc$ (E_{ox} = 0.37 V vs SCE) and [C_5H_4(*n*-Bu)]$_2$Fc (E_{ox} = 0.31 V vs SCE) to TolSQ in the presence of 5.0×10^{-2} M of His·$2H^+$ (E_{red} = 0.29 V vs SCE) are still slightly uphill (ΔG_{et} = 0.08 eV and ΔG_{et} = 0.02 eV, respectively), the follow-up disproportionation of the $TolSQ^{\bullet-}$/His·$2H^+$ complex makes the one-electron oxidation of $(C_5H_5)_2Fc$ and [C_5H_4(*n*-Bu)]$_2$Fc undergo to completion.

(63) Marcus, R. A. *Angew. Chem., Int. Ed. Engl.* **1993**, *32*, 1111.

(64) Okamoto, K.; Imahori, H.; Fukuzumi, S. *J. Am. Chem. Soc.* **2003**, *125*, 7014.

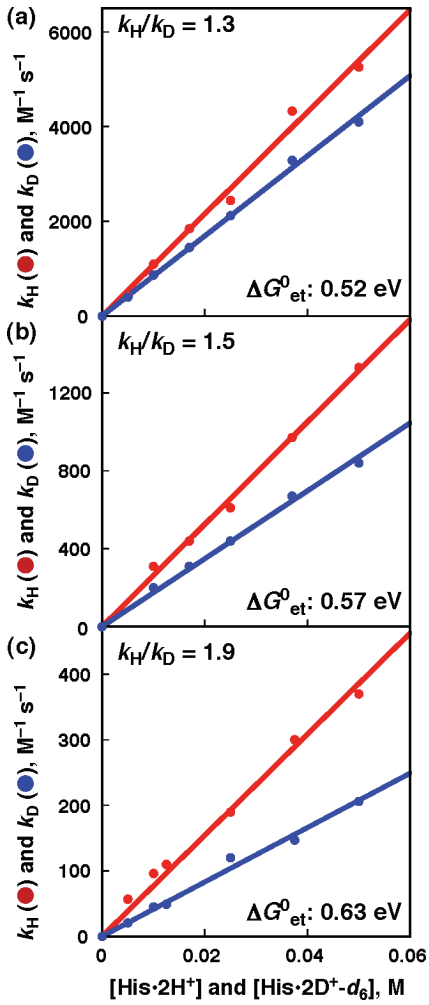

Figure 4. Dependence of k_H (red circles) and k_D (blue circles) on [His·2H$^+$] and [His·2D$^+$-d_6] for ET from (a) $(C_5H_4Me)_2Fc$ (1.0×10^{-4} M), (b) $[C_5H_4(n\text{-Bu})]_2Fc$ (1.0×10^{-4} M), and (c) $(C_5H_5)_2Fc$ (1.0×10^{-4} M) to TolSQ in the presence of His·2H$^+$ and His·2D$^+$-d_6 in deaerated MeCN at 298 K.

ET from R_2Fc to TolSQ (Figure 4 red circles).[65] One may think that the linear correlation of k_H with [His·2H$^+$] (Figure 4) results from the TolSQ/His·2H$^+$ complex (formation constant of TolSQ/His·2H$^+$ is too small to be determined), albeit it was not detected, which increases with increasing the His·2H$^+$ concentration. However, this is certainly not the case of ET reactions,[65] because hydrogen-bond formation of the product of radical anion with the hydrogen-bond donor ($A^{\bullet-}\cdots H^+$:B), which was detected by ESR, results in acceleration of ET (vide supra) without formation of the TolSQ/His·2H$^+$ complex,[10] when the E_{red} value of A is shifted to positive direction.[9,10] This is quite different from the case of the one-step hydride transfer from $AcrH_2$ to TolSQ, which requires formation of the TolSQ/His·2H$^+$ complex prior to the hydride transfer (vide infra).

The rates of ET from R_2Fc to TolSQ exhibit deuterium kinetic isotope effects ($1.3 < k_H/k_D < 1.9$), when His·2H$^+$ is replaced by the deuterated compound (His·2D$^+$-d_6) as shown in Figure 4 blue circles; see the structure of His·2D$^+$-d_6 in eq 3.[66] The observed deuterium kinetic isotope effects may result from partial dissociation of the N−H bond in the hydrogen-bonded

(65) Fukuzumi, S. *Org. Biomol. Chem.* **2003**, *1*, 609.
(66) The deuteration ratio of His·2D$^+$-d_6 was determined to be 98% from the ^{1}H NMR spectrum.

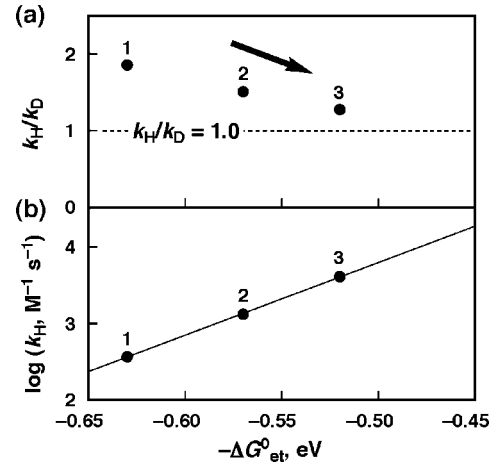

Figure 5. Plots of (a) k_H/k_D and (b) log k_H vs $-\Delta G^0_{et}$ for ET from R_2Fc to TolSQ in the presence of His·2H$^+$ (5.0×10^{-2} M) in deaerated MeCN at 298 K. Numbers at closed circles correspond to Table 1.

NH_3^+ of His·2H$^+$ at the transition state, when the ET is tightly coupled with hydrogen-bond formation (Scheme 5a).[12] The existence of the strong hydrogen bond between $TolSQ^{\bullet-}$ and His·2H$^+$ has been well supported by the existence of the superhyperfine coupling due to the hydrogen-bonded protons and nitrogen of NH_3^+ in the ESR spectrum of $TolSQ^{\bullet-}$/His·2H$^+$ (Figure 1a) (vide supra). The k_H/k_D values for ET from R_2Fc to TolSQ in the presence of His·2H$^+$ (5.0×10^{-2} M) are listed in Table 1 together with the ET driving force ($-\Delta G^0_{et}$) in the absence of His·2H$^+$. The plot of k_H/k_D versus $-\Delta G^0_{et}$ is shown in Figure 5a, combined with the plot of log k_H vs $-\Delta G^0_{et}$ (Figure 5b).[67] The k_H/k_D value decreases with increasing the $-\Delta G^0_{et}$ value to approach $k_H/k_D = 1.0$ (Figure 5a) with a concomitant increase of the log k_H value (Figure 5b).[68] In contrast to the ET coupled with hydrogen-bond formation (Scheme 5a), the rate-determining ET followed by fast hydrogen-bond formation (Scheme 5b) would exhibit no deuterium kinetic isotope effect ($k_H/k_D = 1.0$). Thus, the continuous decrease of the deuterium kinetic isotope effect (k_H/k_D) with an increase in the ET driving force ($-\Delta G^0_{et}$) [Figure 5a] indicates that there is a mechanistic continuity in two reaction pathways, that is, the one-step pathway (Scheme 5a) is continuously changed to the stepwise pathway (Scheme 5b) with increasing the ET driving force ($-\Delta G^0_{et}$). If two reaction pathways were employed simultaneously, the deuterium kinetic isotope effect (k_H/k_D) would be constant irrespective of the ET driving force ($-\Delta G^0_{et}$) above the changeover to the stepwise mechanism (Scheme 5b).[69]

His·2H$^+$ and $HClO_4$-Promoted Hydride Reduction of Quinones by an NADH Analogue. When R_2Fc (electron donor) is replaced by an NADH analogue, $AcrH_2$ ($E_{ox} = 0.81$ V vs SCE)[70] that is a source of two electrons and a proton (equivalent to a hydride ion), no hydride transfer from $AcrH_2$ to TolSQ occurs in the absence of His·2H$^+$. However, an efficient hydride transfer from $AcrH_2$ to TolSQ occurs to yield $AcrH^+$ and $TolSQH_2$ in the presence of His·2H$^+$ (eq 5; for the products analysis, see Experimental Section).[71] The rates of hydride

(67) The k_H/k_D value is plotted against the ET driving force ($-\Delta G^0_{et}$) in the absence of His·2H$^+$, which are highly negative.
(68) The K_1 values are assumed to be the same between the protiated and dueterated His. If the KIE results from the isotope effect in K_1, the KIE value would be constant irrespective of the driving force in contrast to the results in Figure 5. Unfortunately the determination of the K_1 values based on E_{red} values was not accurate enough to recognize a small isotope effect.

Scheme 5. (a) ET Coupled with Hydrogen-Bond Formation; (b) Rate-Determining ET Followed by Fast Hydrogen-Bond Formation

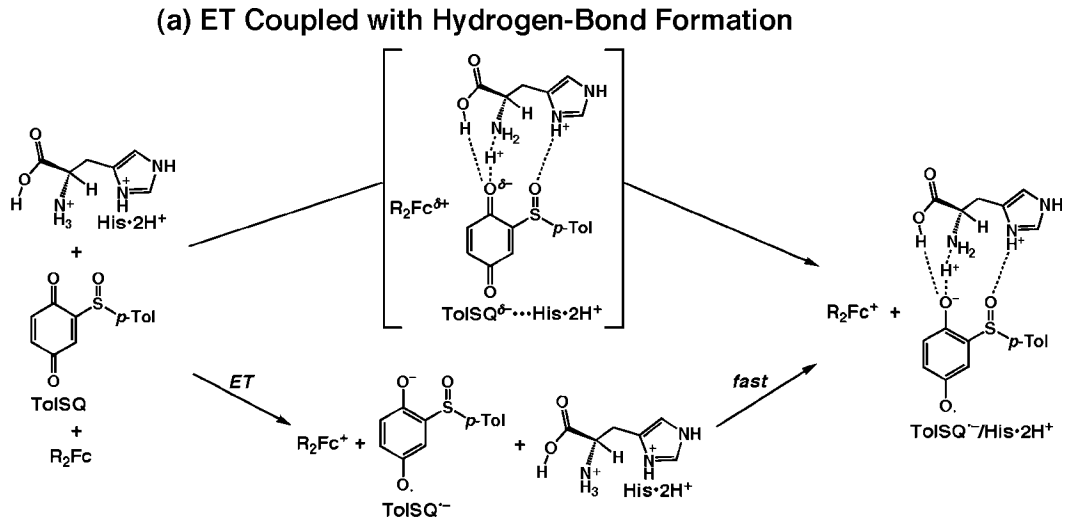

Table 1. One-Electron Oxidation Potentials of R_2Fc (E_{ox}), One-Electron Reduction Potentials of TolSQ in the Absence (E_{red}^0) and Presence of 5.0×10^{-2} M of His·$2H^+$ (E_{red}), Free Energy Change of ET in the Absence (ΔG_{et}^0) and Presence of 5.0×10^{-2} M of His·$2H^+$ (ΔG_{et}), Rate Constants (k_H) of ET from R_2Fc to TolSQ in the presence of His·$2H^+$ (5.0×10^{-2} M), and the Deuterium Kinetic Isotope Effects (k_H/k_D) in Deaerated MeCN at 298 K

no.	R_2Fc	E_{ox} (V vs SCE)	E_{red}^0 (V vs SCE)	E_{red}[a] (V vs SCE)	ΔG_{et}^0 (eV)	ΔG_{et} (eV)	k_H (M^{-1} s^{-1})	k_H/k_D[b]
1	$(C_5H_5)_2Fc$	0.37	−0.26	0.29	0.63	0.08	3.7×10^2	1.9 ± 0.1
2	$[C_5H_4(n\text{-Bu})]_2Fc$	0.31	−0.26	0.29	0.57	0.02	1.3×10^3	1.5 ± 0.1
3	$(C_5H_4Me)_2Fc$	0.26	−0.26	0.29	0.52	−0.03	4.1×10^3	1.3 ± 0.1

[a] Determined by second-harmonic alternating current voltammetry. [b] Determined from the slopes of plots of k_H and k_D vs [His·$2H^+$].

transfer obeyed pseudo-first-order kinetics in the presence of a large excess TolSQ and His·$2H^+$ relative to the concentration of $AcrH_2$ (see the first-order plot in Supporting Information S6).

The observed pseudo-first-order rate constant (k_{obs}) increases proportionally with an increase in [TolSQ] (S7). The second-order rate constant of hydride transfer from $AcrH_2$ to TolSQ with His·$2H^+$ (k_{HH}) also increases linearly with [His·$2H^+$] (red circles in Figure 6a). The rates of hydride transfer exhibit a deuterium kinetic isotope effect ($k_{HH}/k_{DH} = 1.7 \pm 0.1$, when $AcrH_2$ is replaced by the dideuterated compound ($AcrD_2$, k_{DH} denotes the rate constant of hydride transfer from $AcrD_2$ to TolSQ with His·$2H^+$) (blue circles in Figure 6b). In sharp contrast to this, no deuterium kinetic isotope effect ($k_{HH}/k_{HD} = 1.0$ and $k_{DH}/k_{DD} = 1.0$) is observed in hydride transfer from $AcrH_2$ and $AcrD_2$ to TolSQ, when His·$2H^+$ is replaced by His·$2D^+$-d_6 (k_{HD} denotes the rate constant of hydride transfer from $AcrH_2$ to TolSQ with His·$2D^+$-d_6); see red and blue closed triangles in Figure 6, respectively. If the hydride transfer proceeds via ET from $AcrH_2$ ($E_{ox} = 0.81$ V vs SCE)[70] to TolSQ ($E_{red} = -0.26$ V vs SCE) as shown by broken arrow in Scheme 6, the rates of the formal hydride reactions would exhibit deuterium kinetic isotope effects as in the case of His·$2H^+$-promoted ET from R_2Fc to TolSQ (Figure 4), when His·$2H^+$ is replaced by His·$2D^+$-d_6. Thus, the observed deuterium kinetic isotope effect ($k_{HH}/k_{DH} = 1.7 \pm 0.1$) by deuterium substitution of $AcrH_2$ by $AcrD_2$ and the absence of the deuterium kinetic isotope effect ($k_{HH}/k_{HD} = 1.0$ and $k_{DH}/k_{DD} = 1.0$) by deuterium substitution of His·$2H^+$ by His·$2D^+$-d_6 indicate that the hydride transfer proceeds via the one-step pathway (Scheme 6). It should be noted that no absorption band due to $AcrH_2^{\bullet+}$ is observed in the His·$2H^+$-promoted hydride transfer from $AcrH_2$ to TolSQ. The linear correlation between k_{HH} and [His·$2H^+$] (Figure 6a red circles) may result from formation of the hydrogen-bonded

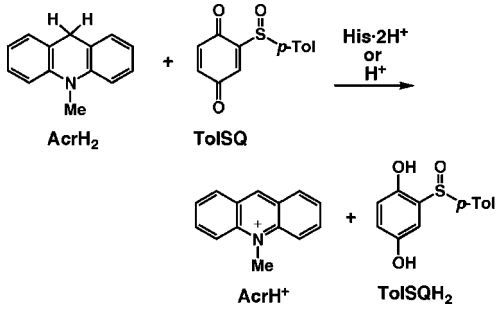

(5)

(69) The ET mechanism would be completely changed to the stepwise pathway (Scheme 5b) with further increasing the ET driving force ($-\Delta G^0_{et}$), in which the rates of ET exhibit no deuterium kinetic isotope effect ($k_H/k_D = 1.0$). However, the rate of such ET with a large driving force was too fast to be determined. In the case of hydride-transfer reactions, the deuterium kinetic isotope effect increases with increasing the driving force when the transition state is productlike or later than symmetirical. In Figure 5, however, the KIE value decreases with increasing the driving force in the region where the driving force is still negative and thereby the transition state is productlike. Thus, the driving force dependence of deuterium kinetic isotope effect for ET from R_2Fc to TolSQ in the presence of His·$2H^+$ (Figure 5) is totally different from the case of hydride-transfer reactions; see: Hermes, J. D.; Morrical, S. W.; O'Leary, M. H.; Cleland, W. W. *Biochemistry* **1984**, *23*, 5479.

(70) Fukuzumi, S.; Ohkubo, K.; Tokuda, Y.; Suenobu, T. *J. Am. Chem. Soc.* **2000**, *122*, 4286.

(71) The stoichiometry in eq 5 and 6 is confirmed by ^{1}H NMR, where 1 equiv of $AcrH_2$ reacts with 1 equiv of TolSQ (or PQ) to yield 1 equiv of $AcrH^+$ and $TolSQH_2$ (or PQH_2) in the presence of His·$2H^+$ (or $HClO_4$).

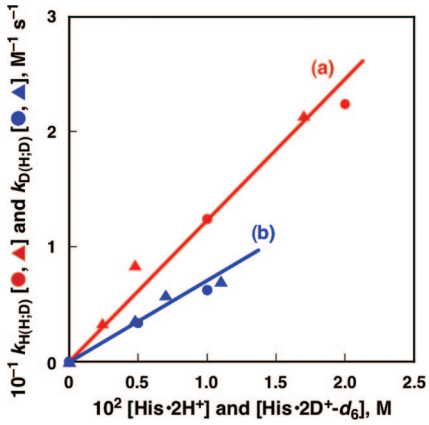

Figure 6. (a) Dependence of k_{HH} (red circles) on [His·2H$^+$] for hydride transfer from $AcrH_2$ (1.0×10^{-4} M) to TolSQ in the presence of His·2H$^+$, and that of k_{HD} (red triangles) on [His·2D$^+$-d_6] for hydride transfer from $AcrH_2$ (1.0×10^{-4} M) to TolSQ in the presence of His·2D$^+$-d_6 in deaerated MeCN at 298 K. (b) Dependence of k_{DH} (blue circles) on [His·2H$^+$] for hydride transfer from $AcrD_2$ (1.0×10^{-4} M) to TolSQ in the presence of His·2H$^+$, and that of k_{DD} (blue triangles) on [His·2D$^+$-d_6] for hydride transfer from $AcrD_2$ (1.0×10^{-4} M) to TolSQ in the presence of His·2D$^+$-d_6 in deaerated MeCN at 298 K.

Scheme 6

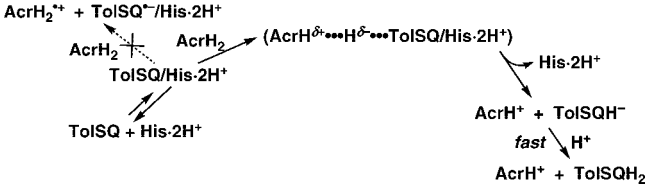

complex between TolSQ and His·2H$^+$ (TolSQ/His·2H$^+$) which increases with increasing the His·2H$^+$ concentration.[65,72]

On the other hand, $HClO_4$ also promotes reductions of TolSQ and PQ by $AcrH_2$, however, the mechanism of this is quite different from that of His·2H$^+$-promoted hydride transfer from $AcrH_2$ to TolSQ (Scheme 6) (vide infra). Efficient reductions of TolSQ and PQ by $AcrH_2$ also occur in the presence of $HClO_4$ (eq 5 and 6, respectively),[73] whereas no hydride reduction occurs in the absence of $HClO_4$.

Stoichiometry of eq 5 is confirmed by the spectral titration of TolSQ by $AcrH_2$ in the presence of $HClO_4$ (Figure 7a), in

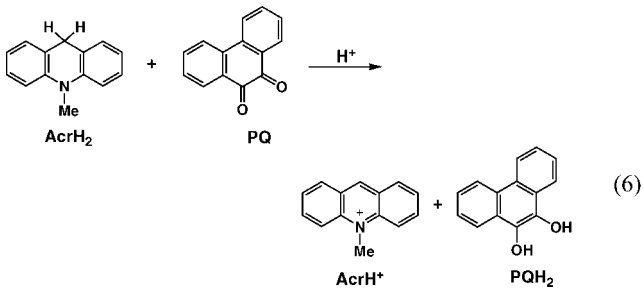

(6)

which all TolSQ molecules are consumed by addition of 1 equiv of $AcrH_2$ to yield 1 equiv of AcrH$^+$.[32,71] The promoting effects of $HClO_4$ on reductions of TolSQ and PQ by $AcrH_2$ should result from protonation of TolSQ (TolSQH$^+$) and PQ (PQH$^+$), and protonation of which is confirmed by UV–vis spectral changes of TolSQ and PQ in the presence of various concentrations of $HClO_4$, respectively (see Supporting Information S8).

The dynamics of the reductions of TolSQ and PQ by $AcrH_2$ were examined by using a stopped-flow technique (vide infra). Stopped-flow mixing of a deaerated MeCN solution of $AcrH_2$ (1.2×10^{-2} M) and that of TolSQ (9.2×10^{-4} M) containing $HClO_4$ (9.8×10^{-2} M) results in instant appearance of a transient absorption band at $\lambda_{max} = 640$ nm (Figure 7b red line),[32] which is ascribed to formation of $AcrH_2^{\bullet+}$ that had been fully characterized including the ESR detection.[29a] To make sure of this, $AcrH_2^{\bullet+}$ have also been detected by applying a rapid-mixing ESR technique in the thermal oxidation of $AcrH_2$ (2.9×10^{-3} M) with TolSQ (2.8×10^{-3} M) in the presence of $HClO_4$ (7.0×10^{-2} M). The resulting ESR spectrum (Figure 7c) can be well reproduced by the computer simulation spectrum (Figure 7d) with the previously reported hfc values [a_H (C-9) = 24.2, a_N (N-CH$_3$) = 14.0, a_H (N-CH$_3$) = 10.4, a_H (C-2,7) = 3.4, and a_H (C-4,5) = 1.0 G] due to $AcrH_2^{\bullet+}$.[29a,74] This strongly supports the formation of $AcrH_2^{\bullet+}$ in the reduction of TolSQH$^+$ by $AcrH_2$. Instant appearance of the transient absorption band due to $AcrH_2^{\bullet+}$ is also observed, when PQ is employed instead of TolSQ (Figure 7e red line). Formation of $AcrH_2^{\bullet+}$ clearly indicates the occurrence of ET from $AcrH_2$ to TolSQH$^+$ and PQH$^+$ (Scheme 7 paths a and b, respectively). No ET from $AcrH_2$ ($E_{ox} = 0.81$ V vs SCE)[70] to TolSQ ($E_{red} = -0.26$ V vs SCE) and PQ ($E_{red} = -0.65$ V vs SCE)[59] occurs in the absence of $HClO_4$, as expected from the highly positive free energy changes of ET ($\Delta G_{et} = 1.07$ and 1.46 eV, respectively). However, the E_{red} values of TolSQ and PQ are shifted to 0.69 and 0.51 V vs SCE, respectively, in the presence of $HClO_4$ (5.0×10^{-2} M) (vide supra). The free energy changes of ET from $AcrH_2$ to TolSQH$^+$ and PQH$^+$ are still slightly positive (ΔG_{et}: 0.12 and 0.30 eV, respectively), which implies occurrence of the subsequent chemical processes. The efficient ET from $AcrH_2$ to TolSQH$^+$ may be followed by rapid disproportionation of TolSQH$^\bullet$ (Scheme 7a, green arrow), which makes ET oxidation of $AcrH_2$ undergo to completion. The absence of ESR signal due to TolSQH$^\bullet$ (Figure 7c) suggests occurrence of rapid disproportionation of TolSQH$^\bullet$ that is produced by ET from $AcrH_2$ to TolSQH$^+$.

In the case of the reduction of TolSQH$^+$ by $AcrH_2$ (Scheme 7a), the absorption at 640 nm due to $AcrH_2^{\bullet+}$ decays accompanied by the rise in absorption at 420 nm due to AcrH$^+$ as shown in Figure 7b (red line−blue line).[32,75] The resulting $AcrH_2^{\bullet+}$ decays (and AcrH$^+$ rises) through both first-order and second-order processes (red and blue circles in inset of Figure 7b), which correspond to the deprotonation and disproportionation of $AcrH_2^{\bullet+}$ as shown by blue and red solid arrows in Scheme 7a, respectively.[32,76] There are large primary kinetic isotope effects in both the first-order and second-order processes ($k_H/k_D = 3.2$ and 10, respectively), when $AcrH_2$ is replaced by

(72) TolSQ/His·2H$^+$ could not be detected, because the formation constant of the TolSQ/His·2H$^+$ complex is too small to be detected (vide supra).

(73) Virtually no protonation of $AcrH_2$ occurs in the presence of $HClO_4$ (4.9×10^{-2} M) containing 30% water. Even when higher concentration of $HClO_4$ was employed in this system, protonation of $AcrH_2$ hardly occurred in the presence of water in MeCN. Nevertheless, protonated NADH analogues are generally still capable of donating electrons to quinones, when the resulting semiquinone radical anion (Q$^{\bullet-}$) is stabilized by the protonation (QH$^\bullet$) [see ref 3,4].

(74) It should be noted that water contained in $HClO_4$ (70%) significantly reduces the sensitivity of ESR.

(75) The differential absorption spectra were recorded by subtracting the final absorption spectrum from the observed spectra during the reduction of TolSQH$^+$ by $AcrH_2$ as shown in Figure 7b. Thus, formation of AcrH$^+$ is represented by the disappearance of the negative absorption band due to AcrH$^+$ (red line−blue line).

(76) Virtually the same first-order and second-order processes were observed in the decay dynamics of $AcrH_2^{\bullet+}$ produced by the ET oxidation of $AcrH_2$ by one-electron oxidants; see: ref 29a.

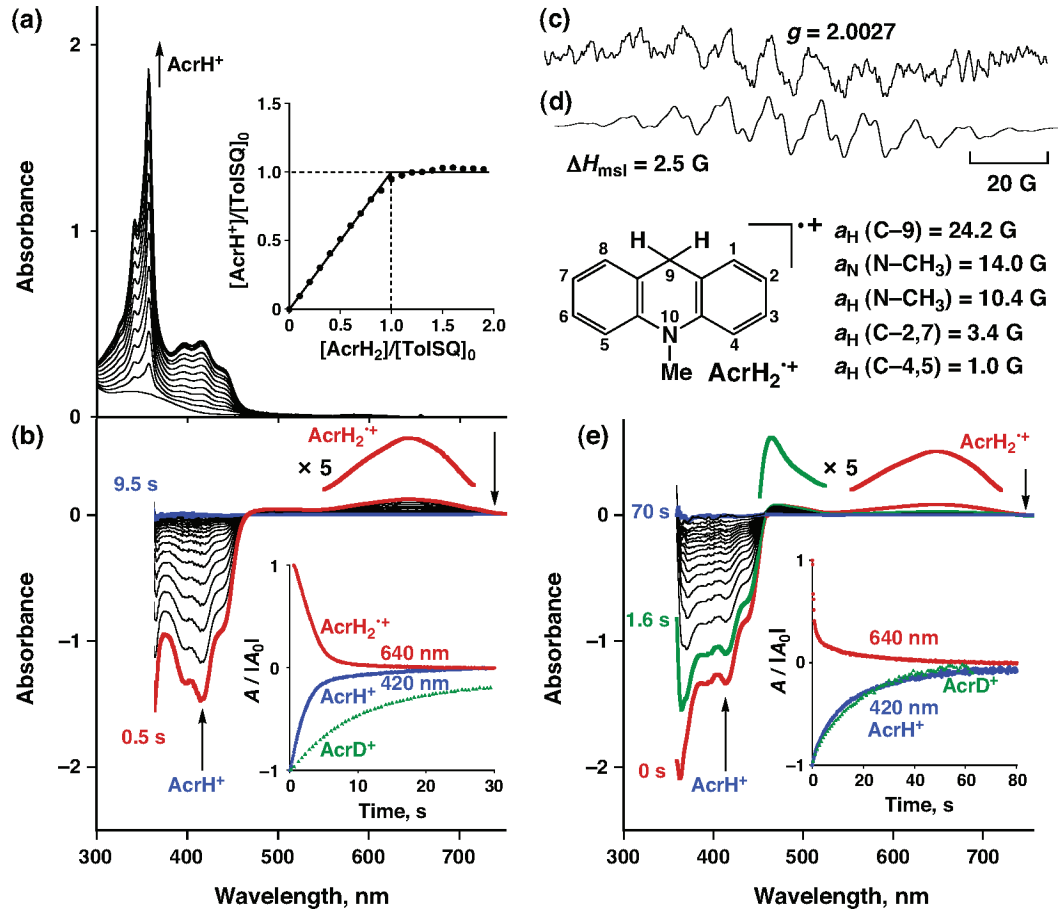

Figure 7. (a) Absorption spectral changes observed upon addition of $AcrH_2$ (0 to 1.9×10^{-4} M) to a deaerated MeCN solution of TolSQ (1.0×10^{-4} M) in the presence of $HClO_4$ (1.0×10^{-1} M) at 298 K. (b) Differential spectral changes in the reduction of TolSQ (4.6×10^{-4} M) by $AcrH_2$ (6.0×10^{-3} M) in the presence of $HClO_4$ (4.9×10^{-2} M) in deaerated MeCN at 298 K. (c) ESR spectrum of $AcrH_2^{\bullet+}$ generated by oxidation of $AcrH_2$ (2.9×10^{-3} M) with TolSQ (2.8×10^{-3} M) in the presence of $HClO_4$ (7.0×10^{-2} M) in deaerated MeCN at 298 K and (d) the computer simulation spectrum. (e) Differential spectral changes in the reduction of PQ (4.9×10^{-4} M) by $AcrH_2$ (4.8×10^{-3} M) in the presence of $HClO_4$ (4.9×10^{-2} M) in deaerated MeCN at 298 K. Insets: (a) Plot of $[AcrH^+]/[TolSQ]_0$ vs $[AcrH_2]/[TolSQ]_0$, where $[TolSQ]_0$ is the initial concentration of TolSQ (1.0×10^{-4} M); time course of the absorption change at $\lambda = 640$ nm (red) and $\lambda = 420$ nm (blue and green) for the reduction of (b) TolSQ and (e) PQ by $AcrH_2$ (red and blue circles) and $AcrD_2$ (green triangles). A_0 = the initial absorbance.

$AcrD_2$ (green triangles in inset of Figure 7b)[32,77] Since $AcrH^{\bullet}$ that is formed by deprotonation of $AcrH_2^{\bullet+}$ (Scheme 7a, blue arrow) acts as a much stronger reductant than $AcrH_2$, the rapid ET from $AcrH^{\bullet}$ ($E_{ox} = -0.46$ V vs SCE)[70] to $TolSQH^+$ occurs to yield $AcrH^+$ and $TolSQH^{\bullet}$ (black solid arrow in Scheme 7a). As a result, 1 equiv of $TolSQH^+$ is reduced by 1 equiv of $AcrH_2$ to yield 1 equiv of $AcrH^+$ and $TolSQH_2$ (Scheme 7a). The proton transfer from $AcrH_2^{\bullet+}$ to $TolSQH^{\bullet}$ (red broken arrow in Scheme 7a) is unlikely to occur, because no protonation of $TolSQH^{\bullet}$ takes place even in the presence of the extremely high concentration of $HClO_4$ as shown in Figure 1g (vide supra).

In contrast to the reduction of $TolSQH^+$ by $AcrH_2$, the absorbance at 640 nm due to $AcrH_2^{\bullet+}$ decays immediately (red circles in inset of Figure 7e) in the reduction of PQH^+ by $AcrH_2$ (Scheme 7b). This does not coincide with the slower rise in absorbance at 420 nm due to $AcrH^+$ (blue circles in inset of Figure 7e) in the reduction of PQH^+ by $AcrH_2$. In such a case, the absorption band at 640 nm due to $AcrH_2^{\bullet+}$ (red line in Figure 7e) is rapidly replaced by the absorption band at 469 nm (green line in Figure 7e) prior to appearance of the absorption band at 420 nm due to $AcrH^+$. This suggests that an adduct between $AcrH_2^{\bullet+}$ and $PQH^{\bullet}$ (or $PQH_2^{\bullet+}$), AcrH-PQH, is initially formed prior to formation of the final products (green arrow in Scheme 7b).[78–81] Such an adduct formation of an NADH analogue with a *p*-quinone derivative has been reported previously in cycloaddition of 1-benzyl-4-*tert*-butyl-1,4-dihydronicotinamide with *p*-benzoquinone.[82] The decay time profile of $AcrH_2^{\bullet+}$ (red circles in inset of Figure 7e) obeys second-order kinetics, exhibiting a

(77) The first-order decay rate constant (k_1) and the second-order decay rate constant of $AcrH_2^{\bullet+}$ (k_2) were determined as 1.1×10^{-1} s^{-1} and 6.6×10^3 M^{-1} s^{-1} from the first-order and second-order plots, respectively (see Supporting Information S9).

(78) Although the transient adduct (AcrH-PQH) could not be fully characterized, Scheme 7b seems to be the most likely mechanism of the reduction of PQH^+ by $AcrH_2$, judging from other NADH model reactions with quinones.[3,4,82].

(79) The optimized structure of AcrH-PQH was obtained by DFT calculations with the BLYP/6-31G** basis set, where the long bond length (1.68 Å) is found between AcrH and PQ moieties (see Supporting Information S11).

(80) The slower decay of absorbance changes at 640 nm (red circles in inset of Figure 7e) may result from the decay of AcrH-PQH that has a small absorption band at 640 nm. Time constant of the slower decay of absorbance changes at 640 nm is therefore quite similar to that of formation of $AcrH^+$ (blue circles in inset of Figure 7e).

(81) The absence of induction period in the formation of $AcrH^+$ (blue circles in inset of Figure 7e may be ascribed to the deprotonation and disproportionation of $AcrH_2^{\bullet+}$ prior to formation of the transient adduct (AcrH-PQH).

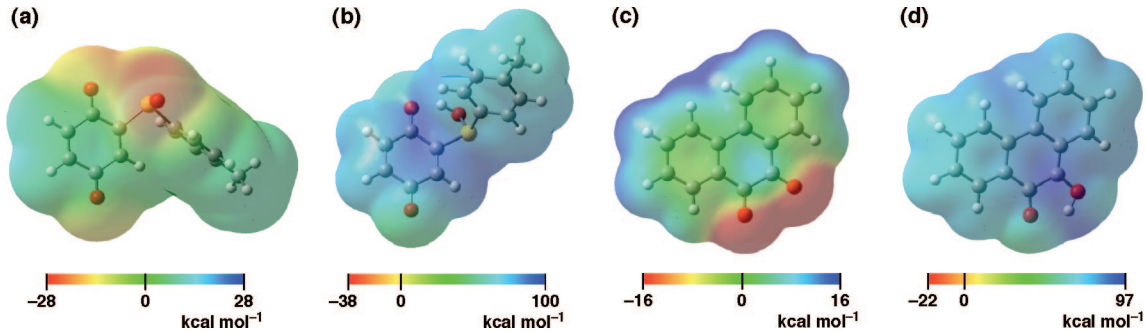

Figure 8. Electrostatic potential maps for (a) TolSQ, (b) $TolSQH^+$, (c) PQ, and (d) PQH^+, calculated by using the density functional theory at the BLYP/6-31G** level.

Scheme 7

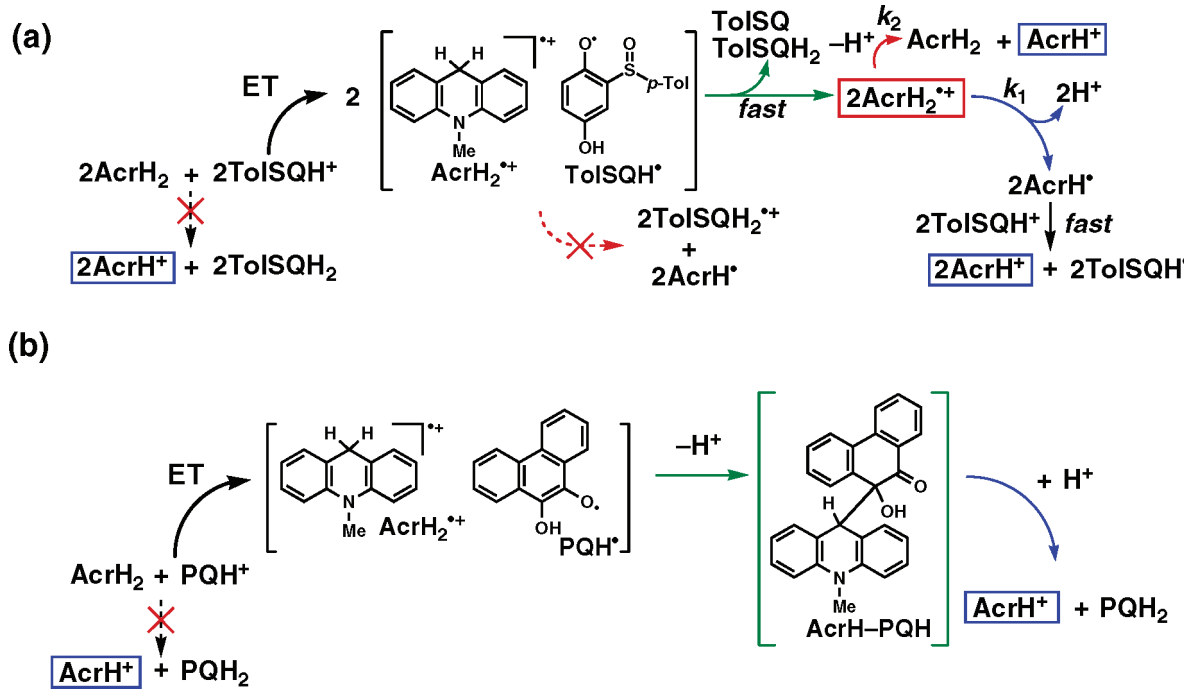

deuterium kinetic isotope effect ($k_H/k_D = 1.5$) (see Supporting Information S10). The observation of the deuterium kinetic isotope effect indicates that deprotonation of $AcrH_2^{\bullet+}$ is involved in the adduct formation (green arrow in Scheme 7b). Heterolysis of AcrH-PQH (blue arrow in Scheme 7b) affords the final products, $AcrH^+$ and PQH_2.[79,83] In fact, the formation dynamics of $AcrH^+$ obeys first-order kinetics without deuterium kinetic isotope effect (blue circles in inset of Figure 7e; see Supporting Information S10).

Protonation of TolSQ and PQ are also expected to result in enhancement of electrophilicity of TolSQ and PQ to accelerate one-step hydride transfer from $AcrH_2$ to $TolSQH^+$ and PQH^+, respectively (Scheme 7 paths a and b, black broken arrows, respectively), as His·$2H^+$-promoted hydride transfer from $AcrH_2$ to TolSQ (Scheme 6). Electrostatic potential maps for $TolSQH^+$ (Figure 8b) and PQH^+ (Figure 8d) indicate that the positive charges (blue) due to protonation of TolSQ and PQ are fully delocalized over the entire ring systems as compared with those of neutral species (Figure 8, panels a and c, respectively).[84] In such a case, the delocalization of the positive charge (due to H^+) in the protonated species ($TolSQH^+$ and PQH^+) does not lead to the expected increase of electrophilicity that would promote the ET pathways, when the E_{red} values of TolSQ and PQ are shifted to the positive direction in the presence of $HClO_4$ (Figure 3, panels e and g, respectively) (vide supra). This may be the reason why ET from $AcrH_2$ to $TolSQH^+$ and PQH^+ (Scheme 7 paths a and b, respectively) occurs instead of the one-step hydride transfer from $AcrH_2$ to $TolSQH^+$ and PQH^+. In the case of His·$2H^+$-promoted hydride transfer, the E_{red} value of TolSQ is also shifted to positive direction (E_{red} = 0.29 V vs SCE) (vide supra). However, the free energy change of ET from $AcrH_2$ (E_{ox} = 0.81 V vs SCE)[70] to TolSQ is still highly positive (ΔG_{et} = 0.52 eV), when the ET reaction is thermodynamically infeasible (broken arrow in Scheme 6).

Summary and Conclusions

We have demonstrated a one-step versus stepwise mechanism in a protonated histidine (His·$2H^+$)-promoted electron-transfer

(82) Fukuzumi, S.; Fujii, Y.; Suenobu, T. *J. Am. Chem. Soc.* **2001**, *123*, 10191.
(83) Heterolysis of AcrH-PQH may be accelerated under acidic conditions.
(84) In contrast to $TolSQH^{\bullet}$, H^+ may be bound to the S=O oxygen, since the larger negative charge (red) is located on the S=O oxygen as compared with the C=O oxygens (Figure 8a).

(ET) reduction of 1-(*p*-tolylsulfinyl)-2,5-benzoquinone (TolSQ) by ferrocenes (R_2Fc) as well as a two-electron reduction by an NADH analogue, 9,10-dihydro-10-methylacridine ($AcrH_2$). Strong hydrogen bonding between the semiquinone radical anion of TolSQ ($TolSQ^{\bullet-}$) and $His\cdot 2H^+$ was revealed by the presence of superhyperfine splitting due to NH_3^+ of $His\cdot 2H^+$ in the ESR spectrum of a hydrogen-bonded complex between $TolSQ^{\bullet-}$ and $His\cdot 2H^+$ ($TolSQ^{\bullet-}$/$His\cdot 2H^+$). Strong hydrogen bonding of $TolSQ^{\bullet-}$ with $His\cdot 2H^+$ results in a large positive shift of the one-electron reduction potential of TolSQ, when ET from R_2Fc to TolSQ becomes possible in the presence of $His\cdot 2H^+$. The ET proceeds in a one-step (concerted) mechanism, that is, ET from R_2Fc to TolSQ is coupled with hydrogen-bond formation of $TolSQ^{\bullet-}$ with $His\cdot 2H^+$. In such a case, the rates of ET exhibit deuterium kinetic isotope effects ($1.3 < k_H/k_D < 1.9$) due to partial dissociation of the N−H bond in $His\cdot 2H^+$ by strong hydrogen bonding of TolSQ with $His\cdot 2H^+$ at the transition state, when $His\cdot 2H^+$ is replaced by the deuterated compound ($His\cdot 2D^+$-d_6). The one-step mechanism, that is, ET coupled with hydrogen-bond formation, is continuously changed to the stepwise mechanism, that is, the rate-limiting ET followed by fast hydrogen-bond formation, with increasing the ET driving force. In such a case, the observed deuterium kinetic isotope effect continuously decreases with increasing the ET driving force to approach $k_H/k_D = 1.0$. On the other hand, $His\cdot 2H^+$ promotes the hydride reduction of TolSQ by $AcrH_2$ via the one-step hydride-transfer mechanism. In such a case, the rates of $His\cdot 2H^+$-promoted hydride transfer exhibit no deuterium kinetic isotope effect, when $His\cdot 2H^+$ is replaced by $His\cdot 2D^+$-d_6, whereas large deuterium kinetic isotope effects are observed, when $AcrH_2$ is replaced by $AcrD_2$. In contrast to $His\cdot 2H^+$-promoted hydride transfer, perchloric acid ($HClO_4$) without His promotes hydride reductions of TolSQ and 9,10-phenanthrenequinone (PQ) by $AcrH_2$ via ET from $AcrH_2$ to $TolSQH^+$ and PQH^+, respectively. Thus, His regulates ET from $AcrH_2$ to $TolSQH^+$, leading to the change of the mechanism of the two-electron reduction of the *p*-quinone derivative (TolSQ) by the NADH analogue ($AcrH_2$) from the ET pathway to the one-step hydride-transfer pathway.

Acknowledgment. This work was partially supported by Grants-in-Aid (No. 19205019) from the Ministry of Education, Culture, Sports, Science and Technology, Japan.

Supporting Information Available: Hydrogen-bond lengths in $TolSQ^{\bullet-}$/$His\cdot 2H^+$ (S1); ESR spectra of $PQD_2^{\bullet+}$ (S2), and $PQH^{\bullet}$ (S3); first-order plot (S4), and dependence of k_{obs} on [TolSQ] (S5) for $His\cdot 2H^+$-promoted ET from R_2Fc to TolSQ; first-order plot (S6) and dependence of k_{obs} on [TolSQ] (S7) for the $His\cdot 2H^+$-promoted hydride reduction of TolSQ by $AcrH_2$; UV–vis spectra of TolSQ and PQ in the presence of $HClO_4$ (S8); first-order and second-order plots for the reductions of TolSQ (S9) and PQ (S10) by $AcrH_2$ and $AcrD_2$; and the optimized structure of AcrH-PQH calculated by DFT at the BLYP/6-31G** level (S11). This material is available free of charge via the Internet at http://pubs.acs.org.

JA8001452